Comparison of rate theories for generalized Langevin dynamics

Susan C. Tucker,[a] Mark E. Tuckerman, and Bruce J. Berne
Department of Chemistry, Columbia University, New York, New York 10027
Eli Pollak
Chemical Physics Department, Weizmann Institue of Science, Rehovot 76100, Israel

(Received 17 June 1991; accepted 12 July 1991)

Rate constants evaluated from (1) the energy-loss turnover theory of Pollak, Grabert, and Hänggi (PGH), (2) the Grote–Hynes extension of Kramers theory (GH), and (3) the microcanonical variational transition state theory for dissipative systems of Tucker and Pollak (μVTST) are compared with rate constants determined from direct computer simulations of generalized Langevin dynamics. The comparisons are made for a cubic oscillator under the influence of a slow bath characterized by a Gaussian friction kernel. In the μVTST calculations, which are based on an effective two degree of freedom Hamiltonian, barrier crossing due to energy transfer from the bath to the effective Hamiltonian is neglected. This neglect is significant only at very strong coupling, where it causes the μVTST results to drop below the simulation results. Both GH and μVTST theories fail (as expected) in the energy diffusion regime, while PGH theory is only moderately successful. The μVTST results agree extremely well with the simulation results in the spatial diffusion regime, providing a significant improvement over the GH results at intermediate coupling strengths and over the PGH results at strong coupling strengths. This improvement is a result of nonlinear effects which are included in the μVTST approach but neglected in the PGH and GH theories.

I. INTRODUCTION

The importance of solvent effects on chemical reactions cannot be disputed, as it is one of the few topics which interests *both* the organic and physical chemist. Of particular interest is the effect of solvents upon the rates of chemical reactions. During the past two decades, a number of theories which incorporate the effects of dissipative media on reaction rate constants have been developed.[1-5] Many of these theories are based upon a generalized Langevin equation (GLE) description of the dynamics, i.e.,

$$m\ddot{q} = -\frac{dW(q)}{dq} - m\int_0^t d\tau\, \gamma(t-\tau)\dot{q}(\tau) + \xi(t), \qquad (1)$$

where q is a one dimensional system coordinate with mass m which is governed by the potential of mean force $W(q)$, the friction kernel $m\gamma(t)$, and the random force $\xi(t)$. The friction kernel determines the total nonisotropic effect of all the bath forces on the system motion. The random force, which is assumed to be a Gaussian random process, averages to zero and satisfies the second fluctuation–dissipation relation,[6]

$$\langle \xi(0)\xi(t)\rangle = mk_bT\gamma(t), \qquad (2)$$

where k_b is Boltzmann's constant and T is temperature.

Generalized Langevin dynamics, while offering the advantage of making very complex problems tractable, only rigorously describes the dynamics of a single degree of freedom (q) of a general $n+1$ ($n\to\infty$) dimensional Hamiltonian in the limit of linear response, i.e., in the limit of infinitesimal variations in the position q.[6] The only exception, i.e., the only case for which the generalized Langevin equation rigorously describes the dynamics for any finite displacement in q, is for the case of a very simple model Hamiltonian in which a bath of n ($n\to\infty$) uncoupled harmonic oscillators x_i are coupled in a bilinear fashion—$V_c = \Sigma_i g_i x_i q$—to the system coordinate q.[7,8] Despite these limitations, theories based on GLE dynamics have been frequently applied to describe reactive motion for realistic molecular Hamiltonians.[9-12]

A common practice has been to test the validity of a given GLE-based theory by applying it to some realistic molecular Hamiltonian and comparing the resultant rate constants to rate constants from molecular dynamics simulations on the same Hamiltonian or from experiment.[9-14] However, because of the limited validity of GLE dynamics—the starting point for these rate theories—such tests are inconclusive. It is impossible to determine whether disagreements between theory and simulation arise because of assumptions made in deriving the theory or because GLE dynamics are simply not valid. Comparison to experiment is even more ambiguous because errors due to inadequacies of the potential are also present to cloud the issue. Even if reasonable agreement is found between theory and simulation or experiment, the number of possible sources of error is such that cancellation of error as the source of agreement is nearly impossible to rule out.

In the current work we present an unambiguous test of three theories based on GLE dynamics—(1) the energy-loss turnover theory of Pollak, Grabert, and Hänggi (PGH),[15] (2) the Grote–Hynes extension of Kramers theory (GH),[16,17] and (3) the microcanonical variational transition state theory for dissipative systems (μVTST) recently introduced by Tucker and Pollak.[18,19] In order to avoid the

---

[a] Current address: Department of Chemistry, University of California, Davis, California 95616.

ambiguity caused by the inapplicability of the GLE for molecular Hamiltonians, the theoretical rate constants are compared to rate constants obtained from a direct simulation of GLE dynamics, rather than from a simulation of molecular dynamics as was done by Straub, Borkovec, and Berne.[12] Thus the comparison of theory with simulation presented here tests the assumptions invoked in deriving rate constant expressions from the GLE. Such direct comparisons to the GLE have been made previously, but only for the restrictive case of exponential friction, see below.[15,24,25] As for the question of the applicability of GLE dynamics to molecular systems, it has recently been addressed elsewhere,[20–23] so it will not be discussed further here.

In order to simulate the GLE, the random force must be sampled in such a way that the second fluctuation–dissipation relation [Eq. (2)] is satisfied. Because an exponential friction kernel, i.e., $\gamma(t) \propto e^{-\alpha t/\tau}$, corresponds to a Markovian random force, sampling of the random force for this kernel is less involved than for an arbitrary friction kernel, and previous comparisons to simulations of GLE dynamics with memory friction have been limited to this specific case.[15,24,25] A method for determining the random force given an arbitrary spectral density was introduced by Rice in 1944[26] and applied to the Langevin equation [$\gamma(t) = \alpha\delta(t)$] in 1945 by Wang and Uhlenbeck.[27] This method was more recently applied to numerical simulations of the GLE with arbitrary friction kernels by McCammon and co-workers.[28] Tuckerman and Berne have further extended this method by combining it with their reference system propagator algorithm (NAPA/RESPA)[29] to allow for efficient simulation when the difference in time scales for the system motion and the bath motion is large.[30] Since friction kernels extracted from molecular dynamics simulations generally look much more like Gaussian than like exponential functions of time,[12,23,31] the ability to simulate GLE dynamics for arbitrary friction kernels is an important advance. It allows one to test the theoretical rate constant expressions under more physically meaningful conditions than when exponential friction is used.

In this work, a cubic oscillator is used to model the one-dimensional reaction potential $W(q)$ and a Gaussian function is used to represent the friction kernel as described in Sec. II. Details of the GLE simulations are given in Sec. III A and the results of the simulations are given in Sec. III B. Special attention is paid to application of the reactive flux method, which allows for efficient calculation of rate constants from the simulation data, to a cubic oscillator governed by GLE dynamics. The three rate theories, PGH, GH, and μVTST, are discussed in Secs. IV–VI, respectively. Each section includes a brief review of the rate theory in Part A and a comparison of the results to the simulation results in Part B. Conclusions follow in Sec. VII.

II. SYSTEM AND PARAMETERS

Specifying a potential of mean force along the system coordinate, $W(q)$, a friction kernel, $\gamma(t)$, and a probability distribution for the random force is sufficient to completely specify a GLE [Eq. (1)]. Here the random force is assumed to be a Gaussian stochastic process. The potential of mean force along the system coordinate is defined in reduced units to be the cubic function

$$W(q) = V^\ddagger - \frac{1}{2}q^2 - \frac{1}{2}q^3 \equiv V^\ddagger - \frac{1}{2}q^2 + V_1, \quad (3)$$

where all frequencies are given in terms of the barrier frequency $\omega^\ddagger$ (thus the reduced barrier frequency is equal to one), and the mass is set to $m = 1$. The cubic oscillator has a minimum at $q = -\frac{2}{3}$ with frequency $\omega_0 = \omega^\ddagger$ and potential $W = 0$ and a maximum at $q = 0$ with potential $W = V^\ddagger = 2/27$ in reduced units. For all computations presented here $\beta(= 1/k_b T)$ is chosen to give a barrier height of $V^\ddagger = 10 k_b T$. This criterion yields $\beta = 135$. For $T = 300$ K this would correspond to a chemically reasonable barrier height of around 6 kcal/mol.

The bath is defined by its friction kernel, which is chosen to be Gaussian in time. As shown by molecular dynamics simulations, a Gaussian friction kernel provides a reasonable representation of a molecular liquid.[12,23,31] The exact form used is, as shown in Fig. 1,

$$\gamma(t) = \sqrt{\frac{2}{\pi}}\,\frac{\alpha}{\tau_D}\,e^{-t^2/2\tau_D^2}, \quad (4)$$

which has the Laplace transform

$$\hat{\gamma}(s) = \alpha e^{(1/2)s^2\tau_D^2}\,\mathrm{erfc}\left(\frac{1}{\sqrt{2}}\,s\tau_D\right). \quad (5)$$

Here the static friction coefficient α [$\hat{\gamma}(0) = \alpha$] controls the strength of the system–bath coupling, erfc is the complementary error function, and the time constant τ_D is roughly a measure of the frequency ratio of the reactive motion to the bath motion. To model the breaking of a chemical bond of a solute molecule in a highly structured liquid, a reactive frequency $\omega^\ddagger$ of 1000 cm^{-1} and an average librational frequency of 100 cm^{-1} are assumed. The value of τ_D for this scenar-

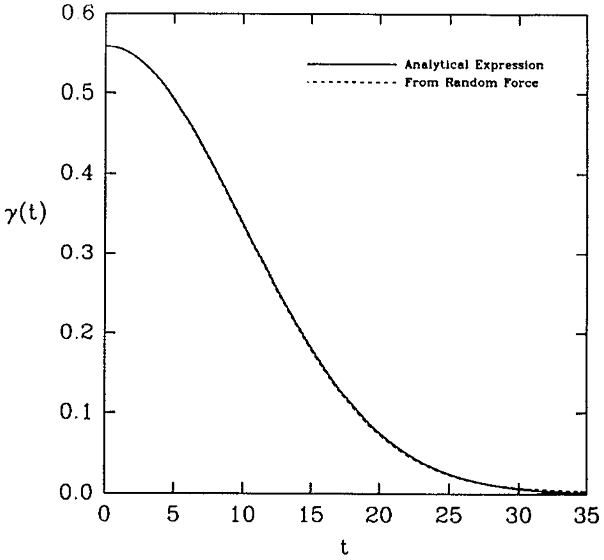

FIG. 1. The Gaussian friction kernel $\gamma(t)$ [Eq. (4)] as a function of time in reduced units (see the text) for a static friction coefficient $\alpha = 7.0$ (also in reduced units). The dashed line is the friction reproduced by the random force in a simulation, see Sec. III A.

io, which is used in all computations presented here, is 10 in units of $1/\omega^\ddagger$.

III. SIMULATIONS

A. Procedure

In order to integrate the GLE for an arbitrary dynamic friction kernel $\gamma(t)$, it must be possible to sample the Gaussian random force. This process is nontrivial because the autocorrelation function of the random force must be proportional to the friction kernel, as given by the fluctuation–dissipation theorem, Eq. (2). A convenient method for sampling the random force is that of Rice,[26] which involves expanding the random force in a Fourier series. The expansion coefficients are sampled from independent Gaussian distributions whose widths are determined from the Fourier cosine transform of the friction kernel. For further details regarding this sampling procedure, see Refs. 28 and 30. As a check on the sampling procedure for the random force, β times the autocorrelation function of the random force from the simulation at $\alpha = 7.0$ is plotted against the analytical friction kernel for $\alpha = 7.0$ in Fig. 1. The agreement, as required by the fluctuation–dissipation theorem [Eq. (2)], is quite good.

Given a method for sampling the random force, the GLE can be integrated to give the progression of q and p_q in time using standard algorithms. It was shown in Ref. 30 that using the velocity Verlet algorithm[32] in combination with the NAPA/RESPA integrator[29] is significantly more efficient than using the velocity Verlet algorithm by itself when there is a significant time scale difference between the system and bath motions. In particular, for the case of an harmonic oscillator of frequency 60 governed by an exponential friction with a decay constant of 0.05, i.e., 3 in units of one over the oscillator frequency, a savings of a factor of 4 in CPU time was achieved by using the NAPA/RESPA method. Here the time scale difference is even larger. The time scale for decay of the friction kernel (the time at half-maximum, see Fig. 1) is 11.8 in units of one over the barrier frequency, and it proves beneficial to use the NAPA/RESPA method.

When calculating rate constants, one is counting occurrences of the rare event of barrier crossing, which happens with probability of order $e^{-\beta V^\ddagger}$. Under the conditions $\beta V^\ddagger = 10$, trajectories would spend an inordinately long time in the well before crossing the barrier, making the computation impractical. To avoid this difficulty we use the reactive flux method.[33,34] The reactive flux method, which was designed for a double well isomerization, can be applied virtually unchanged to the cubic oscillator problem. To evaluate equilibrium rate constants one only needs to consider small displacements in concentration. Thus when evaluating the rate constant for the cubic oscillator, which represents the phenomenology $A \rightarrow B + C$, the rate equations may be linearized, that is

$$\frac{d\delta N_B(t)}{dt} = -[k_f + (N_B^0 + N_C^0)k_b]\delta N_B(t), \qquad (6)$$

where N_X^0 is the equilibrium number of species X, $\delta N_B(t)$ is the deviation in the number of species B at time t from its equilibrium value, k_f is the forward rate constant, k_b is the backward rate constant per unit volume and the term of order $\delta N_B(t)^2$ has been neglected. The phenomenological decay back to equilibrium is then represented by a single exponential with a kinetic rate constant, k_0, which is a sum of the forward rate constant and a pseudo first order backward rate constant,

$$k_0 = k_f + (N_B^0 + N_C^0)k_b. \qquad (7)$$

The reactive flux method gives the ratio of this kinetic rate constant to the conventional transition state theory kinetic rate constant.[35] Since the forward rate constant is proportional to the kinetic rate constant, the reactive flux ratio is also equal to the ratio of the phenomenlogical forward rate constant to the transition state theory forward rate constant.[34]

Application of the reactive flux method to GLE dynamics is relatively straightforward. First, a canonical ensemble of trajectories is found in the conventional dividing surface. For GLE dynamics, this ensemble has $q = 0$ fixed, and the associated momentum $p_q = \dot{q}$ $(m = 1)$ is sampled from the distribution $\dot{q}\Theta(\pm\dot{q})\exp[-\frac{1}{2}\beta\dot{q}^2]$, where Θ is the Heaviside step function.[35] The Gaussian random force is sampled as discussed previously. As these trajectories progress in time (governed by GLE dynamics), one keeps a running ensemble average which keeps track of trajectories which recross the dividing surface. More explicitly this average is, with k the reactive flux and k_{TST} the conventional transition state theory rate constant,[34]

$$\hat{k}(t) = \frac{k(t)}{k_{\text{TST}}} = \int d\Gamma[P^+(\Gamma) - P^-(\Gamma)]\Theta[q(t)], \qquad (8)$$

where

$$P^\pm = \frac{\dot{q}\Theta(\pm\dot{q})\delta(q)e^{-\beta H(\Gamma)}}{\int d\Gamma\, e^{-\beta H(\Gamma)}\dot{q}\Theta(\pm\dot{q})\delta(q)}, \qquad (9)$$

and $\delta(q)$ is the Dirac delta function. For GLE dynamics, Γ represents simply q and p_q. The weight function P^+ (P^-) gives the (normalized) number of trajectories in the dividing surface at time $t = 0$ which are forward (backward) crossing, and Θ is the Heaviside step function, such that

$$\Theta[q(t)] = \begin{cases} 1 & \text{if } q(t) > 0 \text{ (products)} \\ 0 & \text{if } q(t) < 0 \text{ (reactants)} \end{cases} \qquad (10)$$

is a function of time. Clearly, in the limit $t \rightarrow 0$, $\Theta[q(t)]$ is one for all P^+ trajectories and zero for all P^- trajectories, and $\lim_{t\rightarrow 0}\hat{k} = 1$, or $k = k_{\text{TST}}$. Short time transients, i.e., recrossings, will cause oscillations in $\hat{k}(t)$ as it drops to a plateau value $\hat{k}_0$. As the system returns to equilibrium, the plateau decays as the single exponential $\hat{k}_0 e^{-k_0 t}$ with the phenomenological kinetic rate constant k_0. However, in regions of physical interest, this decay generally occurs on a much longer time scale than the short time transients, and the initial plateau value, $\hat{k}_0$, is easily discerned from $\hat{k}(t)$.

The plateau value $\hat{k}_0 = k_{\text{GLE}}/k_{\text{TST}}$ is of interest because it is the ratio of the phenomenological forward rate constant k_{GLE} to the transition state theory forward rate constant k_{TST}. The rate constant k_{TST} is the conventional transition state theory rate constant under the equilibrium solvation assumption. Mathematically, this assumption corresponds to orienting the transition state dividing surface orthogonal to the system coordinate q. As shown by Chandler,[33] under this assumption the conventional transition state theory rate constant can be written in the form of a one-dimensional transition state theory rate constant with the potential replaced by the potential of mean force, i.e.,[36,37]

$$k_{\rm 1DTST}=\frac{\omega_0}{2\pi}e^{-\beta V^\ddagger}, \tag{11}$$

where the harmonic approximation is assumed valid in the reactants region. This one-dimensional transition state theory rate constant is exactly the rate constant to which the rate theories are easily compared.

In the current work, $\hat{k}(t)$ at each value of the static friction coefficient was evaluated from an ensemble of 9000 trajectories. The variance in the plateau value, $\hat{k}_0$, which is evaluated from the binomial distribution of $\Theta[q(t)]$ as in Ref. 24, is 0.005 or less for all values of the static friction considered. All trajectories were run for a total of 409.6 time units with a step size of 0.05 time units. In order to avoid overflow of the cubic potential function at very large positive values of the system coordinate q, trajectories which reached a boundary placed in the products region at $q = 5/6$ were stopped, and thereafter considered to remain in the products region $\{\text{if } q(t_s)\geqslant 5/6, \text{ then } \Theta[t\geqslant t_s]\equiv 1\}$. The value of the potential at $q = 5/6$ is well below the value at the bottom of the well. The simulation results were unaffected by placing the boundary at a larger value of q.

B. Results

Plots of the ratio $\hat{k}(t)$ of the reactive flux to the one-dimensional transition state theory rate constant as a function of time are given in Fig. 2. The function $\hat{k}(t)$ for the cubic oscillator under the influence of a Gaussian friction kernel is shown for three values of the static friction coefficient, $\alpha = 1.0$, 7.0, and 20.0. In the weak coupling limit (small α), recrossings of the dividing surface at $q = 0$ occur because energy deactivation of the trajectories is slower than one traversal of the well. Thus trajectories initially headed towards reactants will return to the barrier with an energy which is still larger than the barrier height, allowing them to recross the dividing surface to products. At $\alpha = 1.0$, there is very little recrossing for the first ~6 time units, the length of time required for one traversal of the well, and $\hat{k}(t)$ drops very little. The following dropoff to the plateau value is very sharp, because most trajectories take a similar length of time to traverse the well. A set of representative trajectories for $\alpha = 1.0$ are shown in Fig. 3. Note that the trajectory which is initially headed toward products does not recross the dividing surface (at $q = 0$), whereas one of those initially headed towards the well does recross the dividing surface once, after nearly a full traversal of the well. The time for this recrossing to occur is indeed around ~6 time units.

In the limit of very strong coupling, on the other hand, recrossings of the dividing surface occur because strong sol-

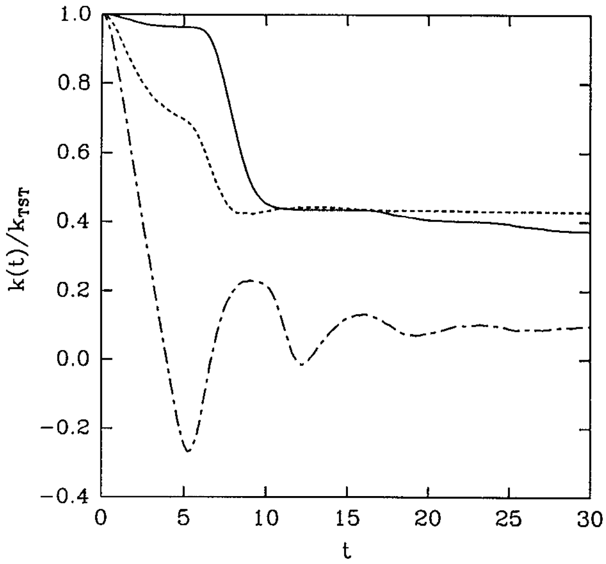

FIG. 2. The ratio, $\hat{k}(t) = k(t)/k_{\rm TST}$, of the reactive flux to the one-dimensional conventional transition state theory rate constant as a function of time for simulations of GLE dynamics. $\hat{k}(t)$ is shown for values of the static friction coefficient (a) $\alpha = 1.0$ (–), (b) $\alpha = 7.0$ (--), and (c) $\alpha = 20.0$ (— -). All quantities are in reduced units, see the text.

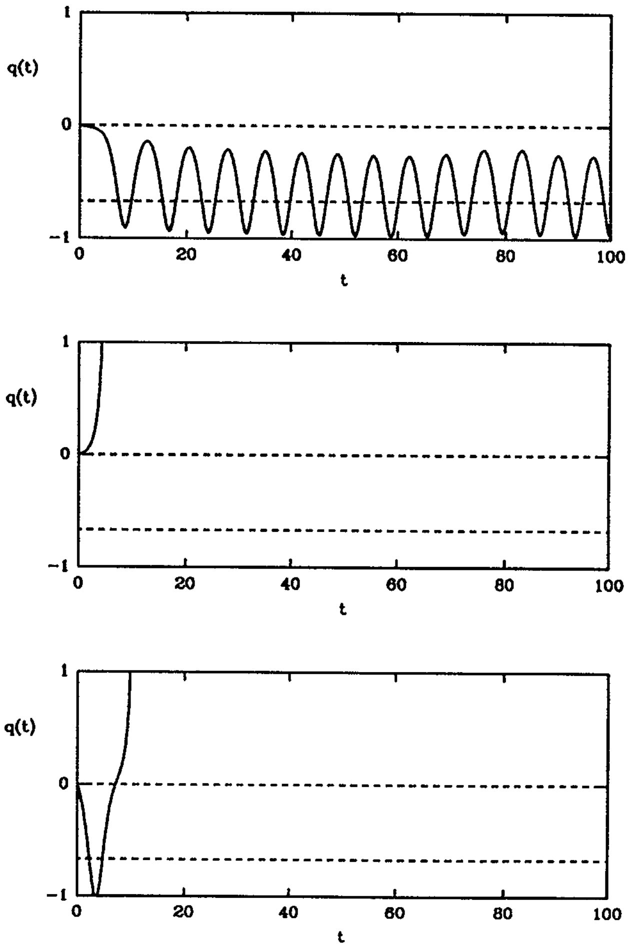

FIG. 3. A representative set of trajectories governed by generalized Langevin dynamics for a cubic potential [Eq. (3)] under the influence of Gaussian friction [Eq. (4)], for a static friction coefficient $\alpha = 1.0$ and a decay time constant $\tau_D = 10$. All trajectories were started at the barrier ($q = 0$). The maximum ($q = 0$) and minimum ($q = -\frac{2}{3}$) of the cubic potential are represented by dashed lines. Time t is given in reduced units, see the text.

vent forces can change the direction of motion of the reactive coordinate q. This limit has been referred to in the literature as the solvent caging regime.[4,9,10,24] In this limit trajectories which are initially headed toward products (dissociation) are just as likely to recross the dividing surface as those initially headed towards reactants (the well), because recrossing is controlled by the solvent forces. For $\alpha = 20.0$ the decay of $\hat{k}(t)$ to its plateau value is very different than the decay at $\alpha = 1.0$. The highly correlated and slowly damped oscillatory behavior is indicative of trajectories which recross the barrier repeatedly with a frequency determined by the solvent forces. Notice that the trajectories for $\alpha = 20.0$ shown in Fig. 4 all oscillate with amplitudes much smaller than the width of the well. Also, trajectories are seen to recross the $q = 0$ dividing surface repeatedly, even the trajectory which eventually relaxes into the well. The damping of the oscillatory signal in $\hat{k}(t)$ occurs as the number of trajectories "trapped" by the "solvent cage" decreases, i.e., the number of trajectories which continue to recross the $q = 0$ dividing surface decreases. Further exploration of the solvent caging effect is presented in Appendix A. Negative values of $\hat{k}(t)$ indicate simply that the contribution of P^- is greater than that of P^+ in Eq. (8), meaning that, at time t, there are more backward (initially towards reactants) trajectories which are on the products side ($q > 0$) than there are forward (initially towards products) trajectories that are on the product side ($q > 0$).

For intermediate coupling strengths, such as $\alpha = 7.0$, the reactive flux illustrates an admixture of the behaviors seen at low and high coupling strengths. This admixture is also seen in the trajectories, a representative set of which are shown in Fig. 5. Notice that the singly recrossing trajectory resembles those at $\alpha = 1.0$, while the multiply recrossing trajectory is more reminiscent of those at $\alpha = 20.0$.

The plateau values are presented in Fig. 6, which is a plot of various rate constants—normalized to the one-dimensional conventional transition state theory rate constant [Eq. (11)]—as a function of the static friction coefficient α for $\alpha = 0.0$ to $\alpha = 20.0$. These results, as well as the values for $\alpha = 100.0$, are listed in Table I. The plot (Fig. 6) covers a broad range of values of the static friction coefficient, encompassing both the energy diffusion and spatial diffusion regimes.[1-3,15,17,24] From the GLE simulation values, one sees that the Kramers turnover region[1-3,15,17] is between $\alpha = 1.0$ and $\alpha = 5.0$.

Notice in Fig. 6 that the rise and fall of the rate constant is given as a function of static friction coefficient α, which is a measure of the system–bath coupling strength, at fixed fric-

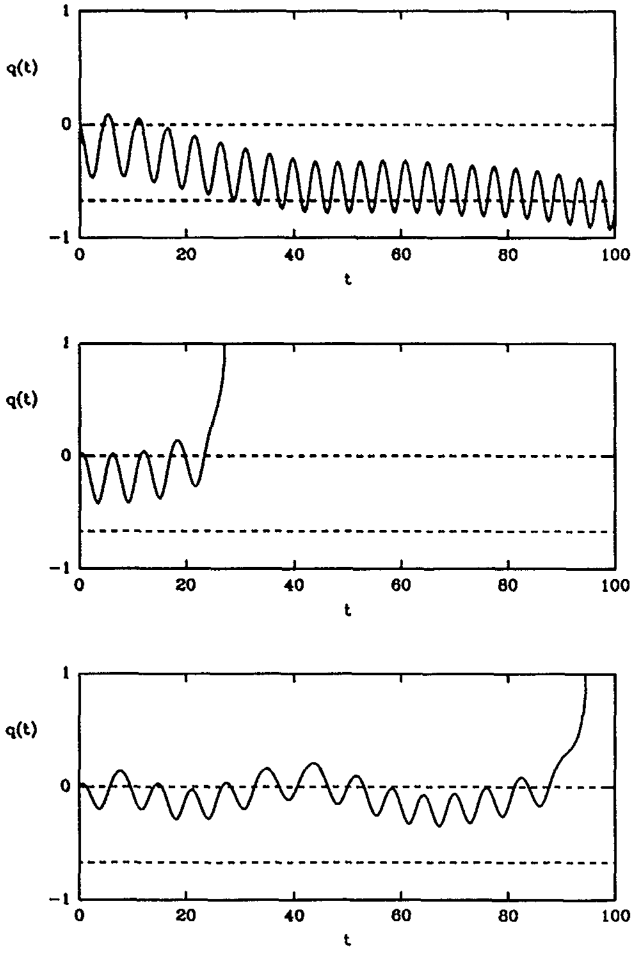

FIG. 4. The same as Fig. 3 except for a static friction coefficient $\alpha = 20.0$.

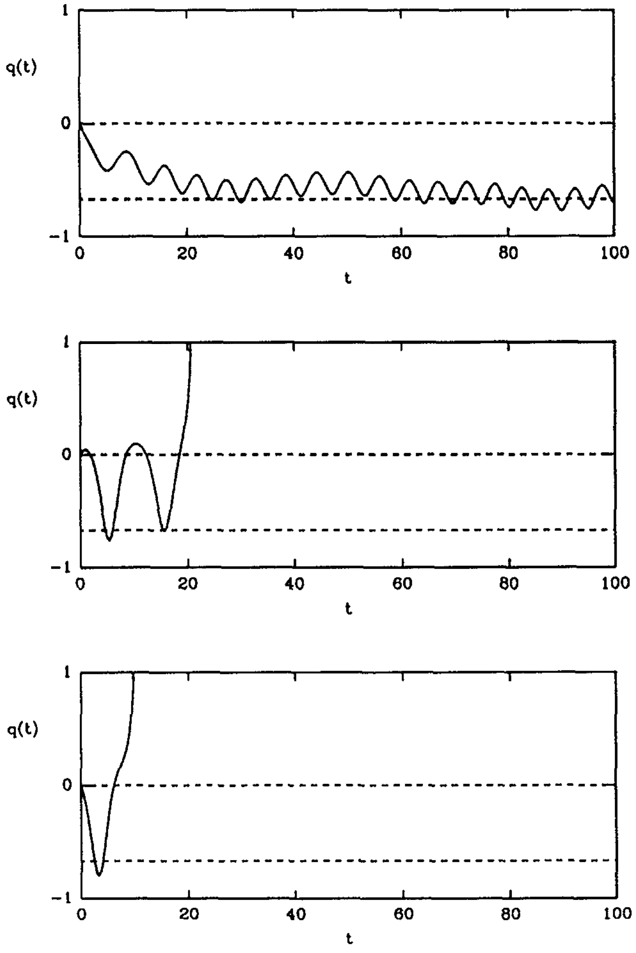

FIG. 5. The same as Fig. 3 except for a static friction coefficient $\alpha = 7.0$.

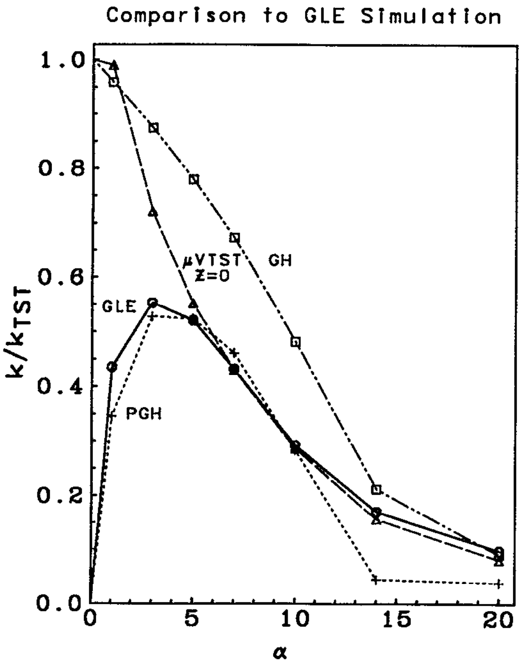

FIG. 6. The ratio of the rate constant from three different calculations to the one-dimensional conventional transition state theory rate constant as a function of the static friction coefficient α (in reduced units). The decay time constant is fixed at a value of $\tau_D = 10$. The solid line gives the GLE simulation results, the short dashed line the PGH results, the dashed line the μVTST results for $\mathscr{I} = 0$ and the patterned dashed line the GH results.

tion decay time constant, τ_D. In the literature, such Kramers plots are also given as functions of a variety of closely related but not necessarily equivalent quantities, such as pressure, viscosity, and damping. In particular, Straub *et al.*,[24] in simulations of rate constants for a bistable well under the influence of an exponential friction kernel, plotted the ratio of k to $k_{\rm TST}$ as a function of the static friction coefficient and the decay time constant. The time constant was related to the static friction coefficient by a simple constant of proportionality; hence as the static friction coefficient was increased, so also was the time constant. Because at high static friction this prescription yields extremely long decay time constants such that the system–bath frequency mismatch hinders energy transfer, Straub *et al.* found the rate to be energy-diffusion limited in this regime. In contrast, in the present work the decay time constant is kept fixed as the static friction coefficient is increased, and no evidence of rate-limiting energy diffusion effects is seen at high static friction.

TABLE I. Ratios of rate constants.

α	$k_{\rm GLE}/k_{\rm TST}$	$k^{\mu\rm VTST}_{\mathscr{I}=0}/k_{\rm TST}$	$k_{\rm PGH}/k_{\rm TST}$	$k_{\rm GH}/k_{\rm TST}$
1.0	0.44	0.99	0.34	0.96
3.0	0.55	0.72	0.53	0.87
5.0	0.52	0.55	0.53	0.78
7.0	0.43	0.43	0.46	0.67
10.0	0.29	0.29	0.28	0.48
14.0	0.17	0.16	0.045	0.21
20.0	0.097	0.080	0.039	0.090
100.0	0.033	0.011	0.010	0.011

In the energy diffusion regime (low static friction, $\alpha < 3.0$) the simulation results rise from a limiting value of zero (not calculated) in the completely uncoupled limit, to a maximum of only ~0.6 in the turnover region (the value at $\alpha = 3.0$, $k_{\rm GLE}/k_{\rm TST} = 0.55$, is not necessarily exactly at the maximum). Simple one-dimensional transition state theory overcounts the rate by 40% at its best.

IV. COMPARISON OF PGH THEORY WITH SIMULATION

A. Review of PGH theory

In 1940 Kramers' original paper[17] provided a challenge to theorists to provide a unified theory which could describe not only the energy diffusion and spatial diffusion regimes, but also the transition between them as a function of the system–bath coupling strength. A number of significant advances have been made toward solving the Kramers turnover problem.[1–4,15,38,39] The most recent of these is the energy-loss turnover theory of Pollak, Grabert, and Hänggi (PGH),[15] a GLE based theory for the escape rate of a particle from a metastable well. PGH theory is based on the idea that motion along the unstable normal coordinate at the saddle point—which is given by a linear combination of both system and bath coordinates—is more important for determining the escape dynamics than is the system coordinate itself.

The GLE, Eq. (1), may be transformed[7,15] into a coupled set of equations of motion for the unstable normal mode ρ and the stable "bath" normal modes $\{y_i\}$, where the coupling is induced by the anharmonic part of the system potential, $V_1(q)$ [Eq. (3)]. Note that the coordinates ρ and $\{y_i\}$ are normal modes at the saddle point ($\rho = 0$, $\{y_i = 0\}$), but are not the normal coordinates elsewhere on the potential unless the anharmonicity $V_1 = 0$. To zero order in the coupling the equation of motion for ρ is

$$\ddot{\rho} - \lambda^{\ddagger 2}\rho = -\frac{\partial V_1}{\partial \rho}(u_{00}\rho), \tag{12}$$

while to first order in the coupling the ith bath mode equation is

$$\ddot{y}_i + \lambda_i^2 y_i = -\frac{u_{i0}}{u_{00}}\frac{\partial V_1}{\partial \rho}(u_{00}\rho), \tag{13}$$

where the eigenvalues, $\lambda^{\ddagger}$, $\{\lambda_i\}$, and eigenvectors, $\mathbf{u}$, of the normal coordinate transformation are defined by the parameters of the GLE.[15] In particular, the unstable normal mode barrier frequency along ρ is[16]

$$\lambda^{\ddagger 2} = \frac{\omega^{\ddagger 2}}{1 + (\hat{\gamma}(\lambda^{\ddagger})/\lambda^{\ddagger})}, \tag{14}$$

and the zero–zero element of $\mathbf{u}$, which measures the ρ–q overlap, is[15]

$$u_{00} = \left[\frac{1}{\epsilon + 1}\right]^{1/2}, \tag{15}$$

where the perturbation parameter ϵ is[15]

$$\epsilon = \frac{1}{2}\left[\frac{\hat{\gamma}(s)}{s} + \frac{\partial \hat{\gamma}(s)}{\partial s}\right]\bigg|_{s=\lambda^{\ddagger}}. \tag{16}$$

The values of the remaining transformation parameters are not needed in practice.

Solving the uncoupled equation (12) for the ρ motion and inserting this into the right-hand side of the stable mode equation (13) enables one to find the solution to the bath equations (13), which, in turn, enables one to evaluate the average energy lost by the ustable mode ρ to the bath during one traversal of the well.[15]

The energy loss is given by the expression[40]

$$\Delta E = \frac{1}{2\pi}\int_{-\infty}^{\infty} ds\,\mathrm{Re}[\hat{K}(is)]f(s). \tag{17}$$

For the cubic oscillator,[40] $f(s)$, which is the square of the Fourier transform of the force on the right-hand side of Eq. (12), is,

$$f(s) = 16\pi^2\left(\frac{\lambda^{\ddagger}}{u_{00}}\right)^6\left[\frac{(s/\lambda^{\ddagger})[(s/\lambda^{\ddagger})^2+1]}{\sinh(\pi s/\lambda^{\ddagger})}\right]^2. \tag{18}$$

For a Gaussian friction kernel [Eq. (4)] the spectral density associated with the bath normal modes, $\mathrm{Re}[\hat{K}(is)]$, is

$$\mathrm{Re}[\hat{K}(is)] = \frac{s^2}{u_{00}^2}\left(\frac{\alpha e^{-(1/2)s^2\tau_D^2}}{\alpha^2 s^2 e^{-s^2\tau_D^2} + \{1 + s^2 - \alpha s(2/\sqrt{\pi})D\,[(1/\sqrt{2})s\tau_D]\}^2}\right), \tag{19}$$

where

$$D(x) = e^{-x^2}\int_0^x dt\, e^{t^2} \tag{20}$$

is Dawson's integral[41] and all other parameters are as previously defined.

From the average energy loss, the conditional probability $P(E\,|E')dE$ that a particle leaving the barrier with energy E' in the ρ mode returns to the barrier with an energy between E and $E + dE$ can be calculated. This conditional probability is then used to construct the steady-state energy distribution in the ρ mode, which can deviate significantly from the equilibrium Boltzmann distribution. Although we do not give the details here,[15] it is important to realize that PGH theory only allows for a nonequilibrium energy distribution for energies within a few $k_b T$ of the barrier—for energies near the well minimum the distribution is assumed to be an equilibrium one. The escape rate is readily evaluated from the probability distribution, since particles reaching the barrier with energy in the ρ mode $E > V^{\ddagger}$ react with probability unity. The resultant expression for the escape rate is[15]

$$k_{\mathrm{PGH}} = f_T k_{\mathrm{1DTST}}, \tag{21}$$

where

$$f_T = \frac{\lambda^{\ddagger}}{\omega^{\ddagger}}\exp\left[\frac{1}{\pi}\int_{-\infty}^{\infty}\frac{dy}{1+y^2}\ln(1 - e^{-\beta\Delta E(1+y^2)/4})\right]. \tag{22}$$

In the reduced units used here, $\omega_0 = \omega^{\ddagger} = 1$ and $\lambda^{\ddagger}$ gives the ratio of the unstable frequency (along ρ) to the barrier frequency (along q). Note that the unstable frequency $\lambda^{\ddagger}$ is exactly the reactive frequency of GH theory (see Sec. V B).[42]

B. Results

The ratio of the rate constants evaluated by PGH theory to the one-dimensional transition state theory rate constants are plotted against the GLE simulation results in Fig. 6. These ratios are also listed in Table I.

In the energy diffusion regime (static friction coefficient $\alpha<3.0$) the PGH theory results correctly show a rise from a limiting value of zero at zero coupling ($\alpha = 0$). However, the PGH rate constant rises too slowly with increasing coupling strength, causing the rate at $\alpha = 1.0$ to be 23% too low. Why is this? Recall that PGH theory assumes an equilibrium energy distribution for energies more than a few $k_b T$ below the barrier height. The full probability distribution is therefore normalized by an equilibrium reactants distribution. If motion in the well is not ergodic, but can be decomposed into regular and irregular regions of phase space, then there will be regions of reactants phase space from which no reactive trajectories will arise.[43,44] In such a situation, normalization of the probability distribution by only those regions of phase space which contribute reactive trajectories would raise the rate constant over the PGH results, since the equilibrium distribution normalization used in PGH theory includes all regions of reactants phase space—both those that do and do not contribute reactive trajectories. Because the GLE simulations were performed by the reactive flux method, which effectively considers only the set of reactive trajectories which actually reach the barrier, the GLE simulation results imply normalization only by those regions of phase space which contribute reactive trajectories. Hence nonergodicity in the reactants region of phase space would cause the PGH results, which assume ergodicity, to fall below the GLE simulation results as observed. In the model problem studied here all intermode coupling is induced by the system anharmonicity, which is quite small near the well minimum,[45] so it is likely that the well phase space will not be ergodic,[46] especially in the weak coupling (energy diffusion) limit.

Another possible explanation for the underestimate of the rate constant by PGH theory in the energy diffusion regime is that the assumption that motion along the ρ mode can be treated only to zero order in the coupling is poor. It is possible that this assumption leads to an underestimate of the energy transfer to the bath. However, it is in the weak coupling energy diffusion regime that this assumption should be the most accurate, while the comparison of the rate constants to simulation show the largest deviation (in the range $1.0\leqslant\alpha\leqslant 10.0$) at the lowest coupling, $\alpha = 1.0$. Furthermore, the perturbation parameter ϵ which provides a measure of the validity of the perturbation theory is significantly less than one for this range of coupling strengths (see

Table II), indicating that perturbation theory should be valid.

At larger values of the static friction coefficient, the PGH results switch from a slight overestimate of the simulation results to a gross underestimate of the simulation results. The poor performance of PGH theory for large values of the static friction coefficient for the system studied here is easily understood. PGH theory is only reliable when the average energy loss is significantly smaller than the barrier height, that is $\Delta E/Q^{\ddagger} \ll 1$, where $Q^{\ddagger}$ is the effective barrier height along the ρ coordinate.[15] For the cubic oscillator under the influence of a Gaussian friction kernel, the effective barrier height along ρ is

$$Q^{\ddagger} = \left(\frac{\lambda^{\ddagger}}{u_{00}}\right)^6 V^{\ddagger}. \tag{23}$$

Note that the effective barrier height along ρ, $Q^{\ddagger}$, can be much smaller than the barrier height along q, $V^{\ddagger}$. The ratio $\Delta E/Q^{\ddagger}$ starts at 0.09 for $\alpha = 1.0$ and increases to 0.99 at $\alpha = 5.0$. This ratio is 2.3 for $\alpha = 7.0$ and 61.9 for $\alpha = 100.0$. Clearly PGH theory is unreliable for $\alpha \sim 5.0$ and larger. Further discussion of the error in PGH theory for strong coupling for the system studied here will be left to Sec. VI B, the discussion of the μVTST results.

V. COMPARISON OF GH THEORY WITH SIMULATION

A. Review of GH theory

The Grote–Hynes extension of Kramers theory (GH),[16,17] is a generalized Langevin equation based rate theory. The GH rate expression, which assumes a parabolic barrier, corrects the one-dimensional transition state theory rate constant for recrossings of the dividing surface caused by the presence of the bath, i.e.,[16]

$$k_{\mathrm{GH}} = \frac{\lambda^{\ddagger}}{\omega^{\ddagger}} k_{\mathrm{1DTST}}, \tag{24}$$

where $\lambda^{\ddagger}$ is the reactive frequency defined by Eq. (14) and k_{1DTST} is given by Eq. (11). In the reduced units used here $\omega^{\ddagger} = 1$ and $\lambda^{\ddagger}$ gives the ratio of the reactive frequency to the barrier frequency. Although the GH expression was not originally derived within a transition state theory formalism, it has been shown to be equivalent to multidimensional conventional harmonic [$V_1 \equiv 0$ in Eq. (3)] transition state theory.[42,47] In conventional transition state theory a planar dividing surface is placed orthogonal to the unbound mode at the saddle point—no optimization of the dividing surface is performed.

TABLE II. The parameters of the reduced two degree of freedom Hamiltonian $H^{\ddagger}$ [Eq. (25)] as a function of the static friction coefficient α, given in reduced units (see the text). $V^{\ddagger} = 2/27$ for all α, $\Delta\Omega^2$ is a measure of energy transfer [Eq. (26)] and ϵ is a measure of the coupling strength [Eq. (16)].

α	$\lambda^{\ddagger 2}$	Ω^2	u_{00}^2	$\Delta\Omega^2$	ϵ
1.0	0.92	0.010	0.999	0.019	0.001
3.0	0.76	0.013	0.996	0.019	0.004
5.0	0.61	0.016	0.990	0.019	0.010
7.0	0.45	0.020	0.976	0.019	0.024
10.0	0.23	0.037	0.894	0.020	0.118
14.0	0.045	0.134	0.285	0.047	2.51
20.0	0.008	0.342	0.031	0.27	31.4
100.0	0.0001	0.847	0.000 26	5.80	3872.

B. Results

The ratios of the GH rate constants to the one-dimensional transition state theory rate constants are shown in Fig. 6 and listed in Table I as a function of the static friction coefficient. The results in the energy diffusion regime (low static friction, $\alpha \leqslant 3.0$) are as expected. The GH theory is a multidimensional transition state theory calculation, and it reduces to the one-dimensional transition state theory result in the limit of zero coupling. Hence, for this theory $k/k_{\mathrm{TST}} = 1$ for $\alpha = 0$. The transition state theory result is incorrect in the weak coupling regime because it assumes an equilibrium canonical distribution of reactant states, when in fact population of states with energy greater than the barrier height is the rate limiting step.[2,5]

As the static friction coefficient is increased, the GH rate constant drops rapidly. This rapid drop in the energy diffusion regime means that multidimensional effects on the spatial diffusion are sizeable even for coupling strengths for which the rate is still controlled by energy diffusion. It is the significant contribution of spatial diffusion effects at weak coupling which causes the low maximum (~ 0.6) in the GLE simulation curve. Despite the rapid drop in the GH rate constant, the GH results are still significantly larger than the simulation results at these intermediate to strong coupling strengths. As stated above, GH theory is a multidimensional TST in which the dividing surface is not optimized. It is the poor choice of dividing surface which causes GH theory to overestimate the rate constant; see Sec. VI B for further discussion of this point.

Finally, at very large coupling strengths ($\alpha = 20.0$), the GH result actually falls below the GLE simulation results. This trend is continued at extremely high coupling, $\alpha = 100.0$ (see Table I). Here the GH result falls ~ 3 times below the GLE simulation result. A poor choice of dividing surface can only raise the value of a transition state theory rate constant.[48,49] Since the GH rate constant is lower than the simulation result, the deviation must be caused by the other main assumption of GH theory, that the anharmonicity V_1 [Eq. (3)] is zero. For a cubic oscillator, inclusion of the anharmonicity would indeed raise the rate constant over the GH (harmonic) value (see Sec. VI B for more detail).[50] The present simulation demonstrates that GH theory does not provide an upper bound to the rate constant in all cases.

VI. COMPARISON OF μVTST WITH SIMULATION

A. Review of μVTST

Like GH theory,[16] μVTST[18] is a multidimensional transition state theory (for reviews of multidimensional transition state theory see, e.g., Refs. 48,49). In contrast to GH theory, μVTST allows for optimization of the dividing surface as a function of energy in a reduced dimensionality space comprised of an unstable mode, ρ, and a collective bath mode, σ. The μVTST also includes the effects of anharmonicity in the system potential by allowing for $V_1 \neq 0$ in Eq. (3). In μVTST the dividing surface is defined by the periodic orbits of a reduced two degree of freedom effective Hamiltonian,

$$H^{\ddagger} = \tfrac{1}{2}p_\rho^2 + \tfrac{1}{2}p_\sigma^2 + V^{\ddagger} - \tfrac{1}{2}\lambda^{\ddagger 2}\rho^2 + \tfrac{1}{2}\Omega^2\sigma^2 + V_1(u_{00}\rho + u_1\sigma), \tag{25}$$

where all parameters are defined in terms of parameters of the GLE [i.e., $W(q),\gamma(t)$]. The unstable normal mode frequency $\lambda^{\ddagger}$ in Eq. (25) is the unstable frequency of PGH theory [Eq. (14)] which is also the reactive frequency of GH theory.[42] The collective bath mode frequency Ω is given by

$$\Omega^2 = \frac{u_1^2}{(u_{00}^2/\lambda^{\ddagger 2}) - (1/\omega^{\ddagger 2})}, \tag{26}$$

where

$$u_1 \equiv [1 - u_{00}^2]^{1/2}. \tag{27}$$

Note that the unstable coordinate ρ of μVTST is exactly the unstable mode ρ of PGH theory; PGH theory is based on a one degree of freedom effective potential, whereas μVTST is based on a two degree of freedom effective potential.

The μVTST rate constant is[18]

$$k^{\mu\mathrm{VTST}} = k_{\mathrm{GH}} \frac{\beta^2\Omega}{2\pi} \int dE^{\ddagger}\, e^{-\beta E^{\ddagger}} F_{\mathrm{tot}}(E^{\ddagger}), \tag{28}$$

where it is assumed that the harmonic approximation is valid in the reactants well. Here $E^{\ddagger}$ is the energy of the reduced Hamiltonian $H^{\ddagger}$, and the flux through the dividing surface at energy $E^{\ddagger}$ is

$$F_{\mathrm{tot}}(E^{\ddagger}) = 2^{3/2}\left(\frac{\beta}{2\pi\Delta\Omega^2}\right)^{1/2} \int d\mathscr{L}\, e^{-(\beta/2)(\mathscr{L}^2/\Delta\Omega^2)} \times \int_{\sigma_<}^{\sigma_>} d\sigma \left[1 + \left(\frac{\partial g}{\partial \sigma} + \mathscr{L}\frac{\partial g}{\partial E^{\ddagger}}\right)^2\right]^{1/2} \times [E^{\ddagger} - V(g,\sigma)]^{1/2}. \tag{29}$$

The sigma integration in Eq. (29) is a line integral along the dividing surface, $g(\sigma,E^{\ddagger})$, at fixed energy $E^{\ddagger}$, and $V(g,\sigma)$ is the potential of the reduced Hamiltonian $H^{\ddagger}$ along $g(\sigma,E^{\ddagger})$ at this energy. The coordinate $\mathscr{L}$ represents energy transfer from the rest of the bath to the collective bath mode σ, and hence to the reduced Hamiltonian $H^{\ddagger}$.[18] The width of the statistical fluctuations which cause this energy transfer is determined by the frequency shift parameter $\Delta\Omega^2$ which is given by

$$\Delta\Omega^2 = \left\{\frac{u_{00}^2}{u_1^2}\frac{2}{\pi}\int_0^\infty ds\, s^2\, \mathrm{Re}[\hat{K}(is)]\right\} - \Omega^2, \tag{30}$$

where the spectral density $\mathrm{Re}[\hat{K}(is)]$ is given in Eq. (19) for a Gaussian friction kernel. Note that $k^{\mu\mathrm{VTST}}$ provides an upper bound to the rate constant (provided that the assumption of harmonic reactants is valid).

As discussed in Ref. 18, $\Delta\Omega^2$ is expected to be small, and hence it is expected that $\mathscr{L} \approx 0$, when there is a large time scale discrepancy between reactive and bath motions. Thus, in the current work, where $\tau_D = 10$, it should be a good approximation to assume that energy transfer contributions to the two degree of freedom Hamiltonian are small and to set $\mathscr{L} = 0$ in the sigma integral. Under this approximation, the flux in Eq. (29) becomes simply the spatial diffusion component, i.e.,

$$F_{\mathrm{tot}}(E^{\ddagger};\mathscr{L}=0) = 2^{3/2}\int_{\sigma_<}^{\sigma_>} d\sigma \left[1 + \left(\frac{\partial g}{\partial \sigma}\right)^2\right]^{1/2} \times [E^{\ddagger} - V(g,\sigma)]^{1/2}, \tag{31}$$

which is also the exact flux expression for the isolated Hamiltonian $H^{\ddagger}$.[18] The periodic orbit dividing surface (pods)[51–54] of $H^{\ddagger}$ at energy $E^{\ddagger}$ is exactly the path which minimizes this flux expression, $F_{\mathrm{tot}}(E^{\ddagger};\mathscr{L}=0)$,[51] and the optimum dividing surface $g(\sigma,E^{\ddagger})$ is thus the set of all pods of the Hamiltonian $H^{\ddagger}$. The approximate rate constant $k^{\mu\mathrm{VTST}}_{\mathscr{L}=0}$ is

$$k^{\mu\mathrm{VTST}}_{\mathscr{L}=0} = k_{1\mathrm{DTST}} \frac{\lambda^{\ddagger}}{\omega^{\ddagger}} \frac{\beta^2\Omega}{2\pi} \int dE^{\ddagger}\, e^{-\beta E^{\ddagger}} F_{\mathrm{tot}}(E^{\ddagger};\mathscr{L}=0). \tag{32}$$

Note that including the energy transfer contributions can only raise the rate constant over the $\mathscr{L}=0$ result, because only trajectories crossing the dividing surface from reactants towards product are counted in the transition state theory formalism.[18]

When the pods of the Hamiltonian $H^{\ddagger}$ are used as the energy dependent dividing surface $g(\sigma,E^{\ddagger})$, the $\mathscr{L}=0$ rate constant, $k^{\mu\mathrm{VTST}}(\mathscr{L}=0)$, may provide a more accurate estimate of the rate constant than the full result including the energy diffusion contribution, $k^{\mu\mathrm{VTST}}$. This is possible because the pods are an optimized dividing surface for the spatial diffusion contribution to the flux but not for the energy diffusion contribution to the flux. Hence, although the spatial diffusion through the pods provides an accurate measure of the spatial diffusion from reactants to products, the energy diffusion through the pods is likely to be an overestimate of the contribution of energy diffusion to the overall flux from the reactants to products. Thus, although the $\mathscr{L}=0$ result is lowered because of the neglected energy diffusion contribution, it may be closer to the true value than is the full result $k^{\mu\mathrm{VTST}}$ if the energy diffusion contribution is greatly overestimated. In order to provide a more accurate result than $k^{\mu\mathrm{VTST}}(\mathscr{L}=0)$, $k^{\mu\mathrm{VTST}}$ [Eq. (28)] would have to be evaluated with a dividing surface $g(\sigma,E^{\ddagger})$ which was optimized to simultaneously minimize the spatial and energy diffusion contributions to $F_{\mathrm{tot}}(E^{\ddagger})$ [Eq. (29)]. Since a practical method for generating this completely optimized dividing surface is not available, we focus on the calculation of the $k^{\mu\mathrm{VTST}}(\mathscr{L}=0)$ for which the optimized surface is known. The full calculations of $k^{\mu\mathrm{VTST}}$ using the pods are presented in Appendix B for comparison.

Contour plots of the reduced dimensionality Hamiltonian $H^{\ddagger}$ for the cubic oscillator under the influence of a Gaussian friction kernel are shown in Fig. 7 for three values of the static friction coefficient, $\alpha = 1.0$, 7.0, and 20.0. Parameters of this Hamiltonian are given in Table II for all values of the static friction coefficient considered. Also given are the parameters $\Delta\Omega^2$, a measure of the neglected energy transfer [Eq. (30)], and ϵ, which is an additional measure of

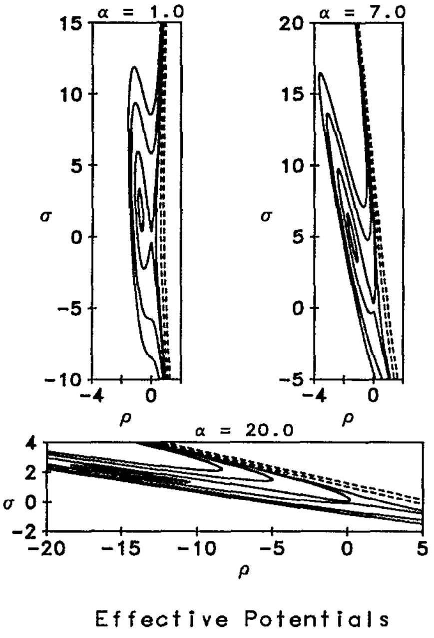

FIG. 7. Contour plots of the reduced two degree of freedom effective Hamiltonian [Eq. (25)] for the cubic potential [Eq. (3)] with a Gaussian friction kernel [Eq. (4)] with decay time constant $\tau_D = 10$ and static friction coefficients of (a) $\alpha = 1.0$, (b) $\alpha = 7.0$, and (c) $\alpha = 20.0$. Contours are at energies -0.6, -0.25 (dashed lines); 0.01, 0.075, 0.25, and 0.45 (solid lines). All quantities are given in reduced units, see the text.

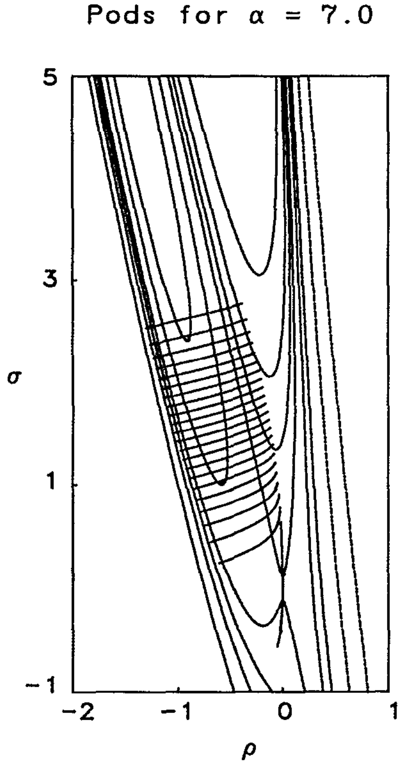

FIG. 8. Periodic orbit dividing surfaces (pods) as a function of the energy of the two degree of freedom effective Hamiltonian [Eq. (25)] for static friction coefficient $\alpha = 7.0$ and decay time constant $\tau_D = 10$. Pods are shown for 25 energies ranging from 0.0741 to 0.1189 by intervals of ~0.001 87. Contour levels are at $E^\ddagger$ equal to -0.2, -0.06 (dashed lines); 0.02, 0.045, 0.0747, 0.09, 0.11, and 0.15 (solid lines). All quantities are given in reduced units, see the text.

coupling strength [Eq. (16)]. For no coupling, $\alpha = 0$, the reduced Hamiltonian would simply be two uncoupled oscillators, a cubic oscillator of frequency $\lambda^\ddagger = \omega^\ddagger$ and a harmonic oscillator of frequency Ω. As the coupling is increased, the frequency $\lambda^\ddagger$ decreases while the frequency Ω increases. The increase in nonlinearity with increasing coupling strength α is illustrated by the increasingly skewed nature of the potential. Note that $\lambda^\ddagger$ and Ω are normal mode frequencies at the barrier, and at large coupling are not the same as the normal mode frequencies in the well. The pods for $H^\ddagger$ for $\alpha = 7.0$ are shown in Fig. 8, for energy $E^\ddagger$ (in reduced units) ranging from 0.074 to 0.1189 in increments of ~0.001 87. Notice that the pods move away from the saddle point as the energy is increased. This behavior is expected because, at higher energies, the available phase space in the barrier region is greatly increased by the anharmonicity in σ, and thus the bottleneck to reaction occurs in the much narrower well region.[52]

It is important to note that for a metastable well pods do not necessarily exist for all energies above the barrier. A pods is only required to exist in (or bounding) the interaction region if there exists both a reactants trap and a products trap.[54] A reactants (products) trap is defined as a region of the potential from which all trajectories proceed to reactants (products). For a metastable well, at high enough energy, trajectories from anywhere in the well can proceed to products, and there exists no well defined reactants trap. Pods are thus not required to exist. For the case at hand, pods are found at all energies needed for convergence of the Boltzmann integral [Eq. (32)] for $\alpha = 10.0$ to $\alpha = 100.0$. For $\alpha \leqslant 7.0$, pods are found to exist for energies from the barrier height to a maximum energy, $E^\ddagger_{\max}$, where $E^\ddagger_{\max}$ is less than the total energy required for convergence of the Boltzmann integral. The value of $E^\ddagger_{\max}$ decreases with decreasing coupling strength. In order to allow for convergence of the Boltzmann integral for each $\alpha \leqslant 7.0$, the pods for $E^\ddagger = E^\ddagger_{\max}$ is used as the dividing surface for all $E^\ddagger \geqslant E^\ddagger_{\max}$. As will be seen in the results, $E^\ddagger_{\max}$ is significantly less than the energy needed for convergence of the Boltzmann integral only for such weak coupling strengths that energy diffusion becomes the rate limiting mechanism for reaction. Transition state theory fails in this regime anyway.

B. Results

Like the GH theory, the μVTST theory is a multidimensional transition state theory calculation, and it reduces to the one-dimensional transition state theory result in the limit of zero coupling. Hence the results are incorrect in the weak coupling limit. In this limit a theory which allows energy transfer to be the rate limiting step, such as PGH theory, is required.

Comparison of the μVTST ($\mathscr{T} = 0$) result to the GH result in the energy diffusion regime (Fig. 6) shows that for $\alpha > 1.0$ the μVTST result drops much more rapidly with increasing static friction than does the GH result. As stated previously, both GH and μVTST are multidimensional transition state theories. However, they differ in that μVTST includes the effect of the anharmonicity of the cubic potential on the rate constant and allows for optimization of the dividing surface in a reduced dimensionality space while GH does neither. For a cubic oscillator, the anharmonicity V_1 [Eq. (3)] is negative and it will therefore cause an increase in the total flux $F_{\rm tot}(E^{\ddagger};\mathscr{L}=0)$ [Eq. (31)] and in the ratio of the μVTST rate constant to the harmonic ($V_1=0$) GH estimate as seen by Eq. (32). For very small coupling strengths ($\alpha\leqslant 1.0$), the optimized dividing surface used in μVTST differs very little from the conventional dividing surface used in GH theory. It follows that the dominant difference between the two rate theories in this regime is the inclusion of anharmonicity, and the μVTST rate constant is larger than the GH rate constant.

For $\alpha > 1.0$ the GH result is larger than the μVTST result, indicating that inclusion of anharmonicity does not dominate the difference between the two theories in this regime. The difference must instead be due to optimization of the dividing surface. Multidimensional transition state theory provides a rigorous upper bound to the rate constant if no approximations are made in the evaluation of the rate expressions.[48,49,51–54] This property allows for variational optimization of the dividing surface, the best dividing surface being that which gives the lowest rate constant, or equivalently, that which gives the minimum flux through itself. Although in μVTST the energy dependent dividing surface is not optimized to minimize the exact flux expression, $F_{\rm tot}(E^{\ddagger})$ [Eq. (29)], at each energy, it is optimized to minimize the exact flux expression, $F_{\rm tot}(E^{\ddagger};\mathscr{L}=0)$ [Eq. (31)], for the effective two degree of freedom Hamiltonian $H^{\ddagger}$. Therefore μVTST would be expected to give a lower rate constant than GH theory, in which no optimization of the dividing surface is performed. From Fig. 6, this is clearly the dominant effect.

In the spatial diffusion regime ($\alpha > 5.0$) there is strikingly good agreement between the μVTST and the GLE simulation results, especially in contrast to the GH results for $\alpha\leqslant 14.0$ (see Table I). In this range of coupling, variational optimization of the dividing surface is clearly necessary for good agreement with the simulation results. It is encouraging that μVTST, which uses a dividing surface optimized for the isolated two degree of freedom effective Hamiltonian $H^{\ddagger}$, is in such good agreement with the simulation results. It is possible that overcounting due to insufficient optimization of the dividing surface is being cancelled by underestimation of the rate due to neglect of energy transfer to the effective Hamiltonian $H^{\ddagger}$ (setting $\mathscr{L}=0$). For $\alpha = 10.0$, an upper bound on the size of the energy transfer contribution is estimated to be about 15% of the $\mathscr{L}=0$ result. This estimate was found by comparing $k^{\mu\rm VTST}$ using the full flux integral $F_{\rm tot}(E^{\ddagger})$ [Eq. (29)] for the pods dividing surface to $k^{\mu\rm VTST}(\mathscr{L}=0)$ [Eq. (32)]. Since the pods dividing surface is not optimized for the energy diffusion contribution, $k^{\mu\rm VTST}/k^{\mu\rm VTST}(\mathscr{L}=0)$ is likely an overestimate of the actual energy diffusion contribution (see Appendix B for details). Also, the width parameter $\Delta\Omega^2$, which controls the amount of energy transfer, is very small, on the order of 0.019 in reduced units for $1.0\leqslant\alpha\leqslant 10.0$ (see Table II). The width parameter is significantly larger than this value for the first time at $\alpha = 14.0$, where $\Delta\Omega^2 = 0.047$, and here the μVTST ($\mathscr{L}=0$) result is slightly lower than the GLE simulation result.

Comparing the μVTST results and the PGH results for intermediate to strong coupling ($5.0\leqslant\alpha\leqslant 10.0$) in Fig. 6 shows that although the PGH results are in very good agreement with the simulation results, the μVTST results are more reliably so. That is, the μVTST curve has the correct curvature (as compared to the GLE results), whereas the PGH results do not, indicating that the accuracy of the PGH results may be somewhat fortuitous.

In Sec. IV B it was suggested that PGH theory is unreliable for $\alpha\geqslant 5.0$ because the effective barrier height along the reactive mode ρ is not substantially larger than k_bT. In Fig. 9, one traversal of the ρ mode well is plotted on the effective two degree of freedom potential used in the μVTST calculations (both quantities are for intermediate coupling strength $\alpha = 10.0$). The ρ mode well is defined simply by setting the value of the collective bath mode σ equal to zero in the two degree of freedom potential. Clearly, the minimum along the ρ mode is much shallower, $Q^{\ddagger} = 0.0013$ or $0.18k_bT$, than the minimum of the well in the two degree of freedom potential. In fact, for the two degree of freedom potential the barrier height relative to the well minimum remains fixed at $V^{\ddagger}$, that is at $10k_bT$ in this case.

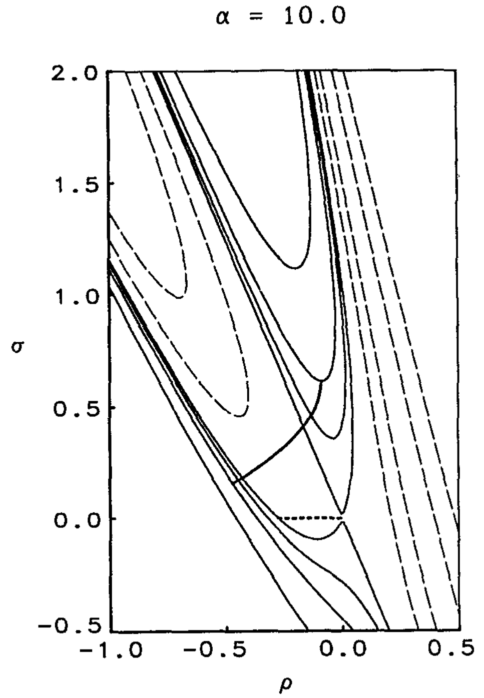

FIG. 9. The periodic orbit dividing surface (pods)—heavy solid line—of the two degree of freedom effective Hamiltonian [Eq. (25)] for static friction coefficient $\alpha = 10.0$, decay time constant $\tau_D = 10$ which gives the maximal contribution to the flux at temperature $\beta = 135$. Also shown is the PGH trajectory along the reactive mode ρ (heavy dotted line). Contour levels are at $E^{\ddagger}$ equal to 0.0, 0.03, 0.055, and 0.065 (dashed lines); 0.074 08, 0.076, 0.079 34, and 0.09 (solid lines). All quantities are given in reduced units, see the text.

Also shown in Fig. 9 is the pods of the effective two degree of freedom Hamiltonian which gives the maximal contribution to the reactive flux for temperature $\beta = 135$. This pods defines a division between reactants and products. From Fig. 9 one sees that the PGH trajectory never traverses the full well; it never even enters the reactants region. PGH theory does as well as it does for $5.0 \leqslant \alpha \leqslant 10.0$ because energy transfer in the well region is very limited,[45,46] and most of the energy transfer actually takes place in the interaction region between the barrier and the well, which is explored by the PGH trajectory. At higher values of the coupling, i.e., $\alpha \geqslant 14.0$, the PGH trajectories no longer explore even the interaction region sufficiently, and the PGH theory rate constants drop significantly below the simulation values. The failure of a perturbation theory based on this one-dimensional model for $\alpha \geqslant 14.0$ is confirmed by the significant increase in the perturbation parameter ϵ to values greater than one at large coupling strengths (see Table II).

In contrast, at very large coupling strengths ($\alpha = 20.0$), the μVTST result is again only slightly lower than the simulation result because of the neglected energy diffusion term. Here the width parameter for the energy transfer is an order of magnitude larger than at lower α's, i.e., $\Delta\Omega^2 = 0.27$. It is not until the extreme value of $\alpha = 100.0$ that the error in the μVTST ($\mathscr{T} = 0$) results approaches that in the PGH results. Here the width parameter is yet another order of magnitude larger, $\Delta\Omega^2 = 5.80$.

VII. CONCLUSIONS

Two multidimensional transition state theories and one energy transfer theory, all of which were derived under the assumption of generalized Langevin dynamics, have been tested against computer simulations of the generalized Langevin equation for a cubic oscillator under the influence of a much slower bath characterized by a Gaussian friction kernel. In particular the microcanonical variational transition state theory for dissipative systems (μVTST) of Tucker and Pollak is considered in comparison to the energy-loss turnover theory of Pollak, Grabert, and Hänggi (PGH) and to the Grote–Hynes extension of Kramers theory (GH). The μVTST theory, which is based on an effective two degree of freedom Hamiltonian with a reactive mode and a collective bath mode, is considered in the limit that barrier crossing induced by energy transfer from the bath to the effective two degree of freedom Hamiltonian is negligible. This should be a good approximation in the case that the time scale of the bath motion is significantly slower than the time scale of the reactive motion, which is the situation studied here.

In the limit of weak coupling, i.e., in the energy diffusion limit, neither transition state theory (GH or μVTST) gives rate constants which agree with the simulation rate constants. This failure is expected, because all transition state theories assume an equilibrium distribution of reactants when, in fact, population of reactants with energy greater than the barrier height is the rate limiting step in this regime. In this regime PGH theory correctly predicts a rise in the rate constant from a value of zero in the limit of no coupling. As compared to the simulation results, however, the PGH rate constant rises too slowly as a function of the coupling strength. This deviation is attributed to a breakdown of the assumption that phase space is ergodic in the well region.

At intermediate to strong coupling, that is, in the spatial diffusion limit, the μVTST rate constants agree almost exactly with the simulation rate constants, indicating that the effective two degree of freedom Hamiltonian is an excellent model for the full dissipative problem. In contrast, the GH rate constants in this coupling regime are nearly a factor of two larger than the simulation and μVTST rate constants. The PGH rate constants agree quite well with the simulation results in this regime, but this may be somewhat fortuitous. The curvature of the plot of the PGH rate constants vs the static friction coefficient (coupling strength) is incorrect as compared to the simulations. This curvature is correct for the μVTST results. Theoretically the PGH results are expected to be unreliable in this regime because the effective barrier height along the reactive coordinate (which is relevant only to PGH theory) is not significantly larger than $k_b T$. Concurrently, the use of a one-dimensional model for the zero order approximation becomes questionable. The two degree of freedom model used in μVTST provides a much better representation at stronger coupling strengths.

PGH theory fails as the coupling is further increased. The one-dimensional model does not provide an adequate description of the dynamics. In contrast, the μVTST rate constant drops only slightly below the simulation rate constant as the neglected energy-transfer-induced barrier crossing ceases to be negligible. The GH results also drop below the simulation results, a sign that, in this regime, the neglect of anharmonicity outweighs the effects of using the conventional dividing surface. Finally, at extremely large coupling, none of the rate theories is in acceptable agreement with the simulation results. They are all significantly low.

The very good agreement of the μVTST results, which are based on a dividing surface which is optimized for the isolated effective two degree of freedom Hamiltonian, to the simulation results in the spatial diffusion regime is significant. The deviation of the GH results indicates that optimization of the dividing surface can be as important in dissipative systems as it has been shown to be in gas phase systems. Yet, from the agreement of the μVTST results, it is clear that the reduced subspace of the effective two-dimensional Hamiltonian allows enough variation for sufficient optimization of the dividing surface.

ACKNOWLEDGMENTS

We would like to thank Kaushik Ghosh for useful discussions on functional analysis and Miguel Sepulveda for providing a trajectory integration subroutine based on the NAG library. This work has been supported by grants from the National Science Foundation (No. CHE-87-00522), the U.S.–Israel Binational Science Foundation and the Petroleum Research Foundation.

APPENDIX A: THE CAGING EFFECT AT LARGE COUPLING

At very large system–bath coupling strengths, motion along the system coordinate q in the barrier region will be highly oscillatory if there is a sufficient time scale disparity between system and bath motion. This highly oscillatory behavior, as illustrated by trajectories with static friction coefficient $\alpha = 100$ (see Figs. 10 and 11) has been referred to in the literature as the solvent caging effect.[4,9,10,24] Below, we show that the observed oscillations along the system coordinate q can be explained both from the traditional caging point of view[4,9,10,24] and from an alternative normal coordinate point of view.[15,55]

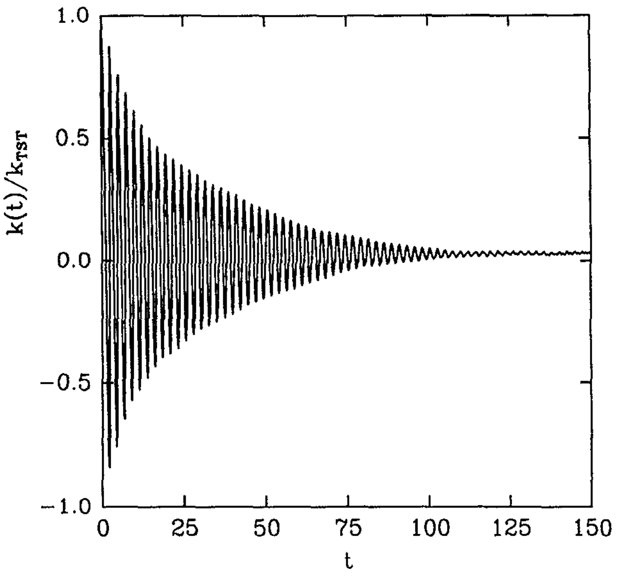

FIG. 11. The ratio $\hat{k}(t) = k(t)/k_{\mathrm{TST}}$ of the reactive flux to the one-dimensional conventional TST rate constant as a function of time for simulation of GLE dynamics with static friction coefficient $\alpha = 100$.

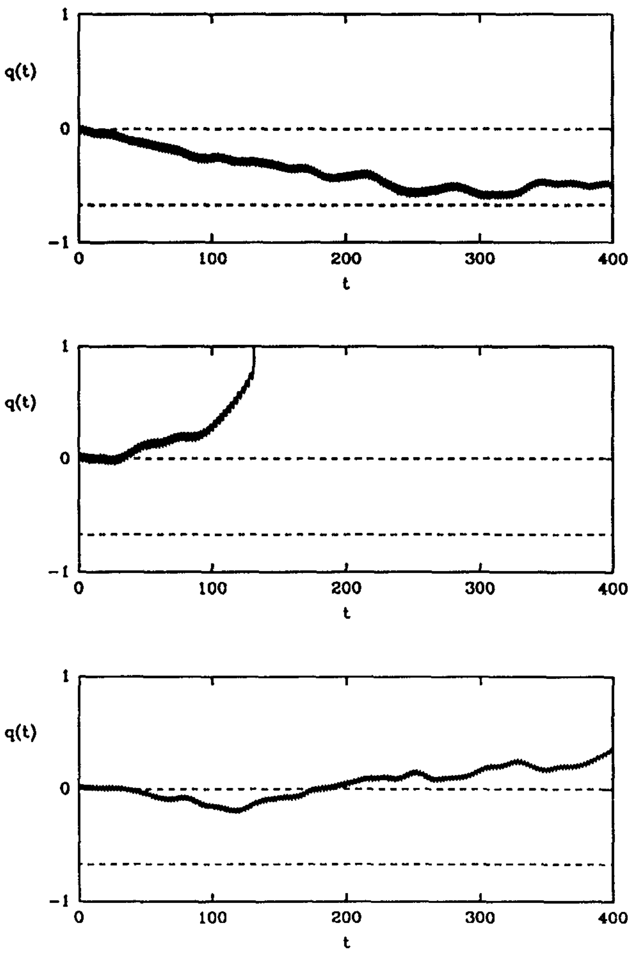

FIG. 10. The same as Fig. 3 except for a static friction coefficient $\alpha = 100.0$.

In the traditional view of solvent caging, the slowly moving solvent is said to form a rigid cage around the dissociating solute. The fast moving solute oscillates many times within this cage before solvent motion breaks the cage and allows for solute dissociation. This view of the system coordinate can be determined from the GLE when the decay of the friction kernel (i.e., the correlation time for the random force) is very slow compared with oscillations in the system motion. First, the GLE is rewritten as

$$m\ddot{q} = -\frac{dW}{dq} + m\gamma(t)q(0) - m\gamma(0)q(t) - m\gamma(0)\int_0^t d\tau\,\frac{\dot{\gamma}(t-\tau)}{\gamma(0)}\,q(\tau) + \xi(t), \qquad \text{(A1)}$$

where the memory integral has been integrated by parts. For the Gaussian friction kernel, given that $q(0) = 0$, the GLE becomes

$$m\ddot{q} = -\frac{dW}{dq} - m\gamma(0)(q(t) - a[q,t]) + \xi(t), \qquad \text{(A2)}$$

where

$$a[q,t] = \frac{1}{\tau_D^2}\int_0^t d\tau\,(t-\tau)e^{-(t-\tau)^2/\tau_D^2}q(\tau). \qquad \text{(A3)}$$

If the decay constant τ_D is large, the contribution from $a[q,t]$ will be negligible since $\dot{\gamma}(t)/\gamma(0)$ goes as $1/\tau_D^2$. Under these conditions the GLE becomes

$$m\ddot{q} \approx -\frac{d}{dq}\left[W(q) + \frac{1}{2}m\gamma(0)q^2\right] + \xi(t), \qquad \text{(A4)}$$

as shown in Ref. 24. The effective potential in the square brackets is plotted along with $W(q)$ in Fig. 12. For the cubic potential with $m = 1$, this effective potential is strongly harmonic around $q = 0$ with a frequency of

$$\omega = [\gamma(0) - 1]^{1/2}, \qquad \text{(A5)}$$

where $\gamma(0) = \sqrt{2/\pi}(\alpha/\tau_D)$. For fixed τ_D, the degree to which the system coordinate q will exhibit high frequency oscillations is determined entirely by α. For small enough α, $\omega^2 < 0$, and q will exhibit the behavior of an unbound mode. For $\alpha = 100$ and $\tau_D = 10$, $\omega = 2.64$, in agreement with the frequency of oscillations seen both in $\hat{k}(t)$ (Fig. 11) and in the simulated trajectories (Fig. 10). However, the approximate GLE in Eq. (A4) predicts that the trajectories would oscillate around $q = 0$ for long times. A closer look at Fig. 10 shows that the high frequency oscillations continue for very long times, but the minimum around which these oscillations occur drifts over time. This drift occurs because $\tau_D = 10$ is not large enough for $a[q,t]$ to be completely neglected.

To understand the effect of $a[q,t]$, an effective potential—which explicitly includes $a[q,t]$—from which the GLE in the form of Eq. (A1) can be derived exactly is considered. The force $m\gamma(0)a[q,t]$ in Eq. (A2) is nonlocal in time and therefore depends on the entire history of $q(t)$. Such a force can only be derived from a nonlocal potential and is thus written as a nonlocal or functional derivative of such a potential with respect to the function $q(t)$. Denoting the nonlocal potential as $\mathscr{W}_{\text{eff}}[q,t]$, the GLE is written in the form

$$m\ddot{q} = -\frac{\delta \mathscr{W}_{\text{eff}}[q,t]}{\delta q(t)} + \xi(t). \tag{A6}$$

In order to find a nonlocal potential which will give back the GLE, the deterministic part of the force on the right-hand side of Eq. (A2) is functionally integrated, giving an effective potential of the form

$$\mathscr{W}_{\text{eff}}[q,t] = \int_0^\infty dz[W(q(z)) + \tfrac{1}{2}m\gamma(0)\{q(z) - a[q,z]\}^2] + \epsilon[q,t], \tag{A7}$$

where $W(q(z))$ is the ordinary potential of mean force, Eq. (1). Note that because $\mathscr{W}_{\text{eff}}[q,t]$ is obtained by functional integration, it has the dimensions of an action. The nonlocality of the effective potential is reflected in the integral over z which is an integral over all time. The additional functional, $\epsilon[q,t]$, is required because the functional derivative of the first term does not yield the GLE exactly. The term $\epsilon[q,t]$ corrects for this. Explicitly, the functional derivative of Eq. (A7) is

$$\frac{\delta \mathscr{W}_{\text{eff}}[q,t]}{\delta q(t)} = \int_0^\infty dz\Big[\frac{\partial W}{\partial q(t)}\delta(t-z) + m\gamma(0)(q(z) - a[q,z]) \times\Big(\delta(t-z) - \frac{\delta a[q,z]}{\delta q(t)}\Big)\Big] + \frac{\delta \epsilon[q,t]}{\delta q(t)}. \tag{A8}$$

If $\epsilon[q,t]$ is chosen such that

$$\frac{\delta \epsilon[q,t]}{\delta q(t)} = \int_0^\infty dz\, m\gamma(0)(q(z) - a[q,z])\frac{\delta a[q,z]}{\delta q(t)}, \tag{A9}$$

$\mathscr{W}_{\text{eff}}[q,t]$ will reproduce the GLE exactly. By functionally differentiating Eq. (A9) with respect to $q(t')$, the second derivative of $\epsilon[q,t]$ can be shown to be independent of q altogether. Thus $\epsilon[q,t]$ can be computed exactly from the functional Taylor series taken out to second order in q. The result is

$$\epsilon[q,t] = -\frac{m}{2}\int_t^\infty dz\int_t^\infty dz'\, q(z)\dot{\gamma}(|z-z'|)q(z') - \frac{m}{2}\int_0^\infty dz\int_0^z d\tau\int_0^z d\tau'\, q(\tau) \times\frac{\dot{\gamma}(z-\tau)\dot{\gamma}(z-\tau')}{\gamma(0)}q(\tau'). \tag{A10}$$

By transforming to dimensionless variables in Eqs. (A7) and (A10), it becomes clear that $\epsilon[q,t]$ is smaller than the harmonic term in Eq. (A7) by a factor of $1/\tau_D$ so that it may be neglected for the purposes of this analysis.

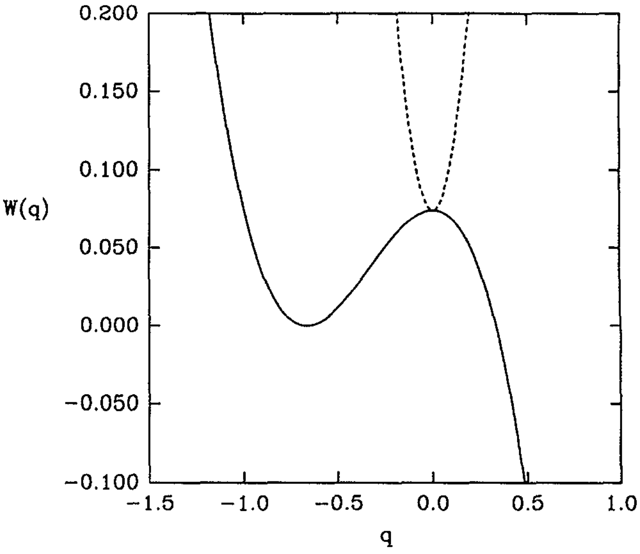

FIG. 12. The effective caging potential as given by Eq. (A4) (dashed line) plotted against the true potential $W(q)$ given by Eq. (3) (solid line). Here, $m = 1$, $\gamma(0) = \sqrt{2/\pi}(\alpha/\tau_D)$, $\alpha = 100$, and $\tau_D = 10$.

Neglecting $\epsilon[q,t]$ is equivalent to neglecting the dependence of $a[q,t]$ on the endpoint of the path (i.e., q at time t). If this approximation is made, then

$$\frac{\delta \mathscr{W}_{\text{eff}}[q,t]}{\delta q(t)} \approx \int_0^\infty dz\frac{\partial}{\partial q(t)}[W(q(z)) + \tfrac{1}{2}m\gamma(0)(q(z) - a[q,z])^2]\delta(t-z) = \frac{\partial}{\partial q(t)}[W(q) + \tfrac{1}{2}m\gamma(0)(q(t) - a[q,t])^2], \tag{A11}$$

where $a[q,t]$ is now assumed to be independent of q at time t. This approximation amounts to replacing the effective nonlocal potential by a local one of the form

$$W_{\text{eff}}(q,t) = W(q) + \tfrac{1}{2}m\gamma(0)(q - a[q,t])^2. \tag{A12}$$

Like the potential in Eq. (A4), the potential in Eq. (A12) has a strong harmonic component for large $\gamma(0)$, but it also has a time-dependent minimum. For the cubic potential of Eq. (3) ($m = 1$), Eq. (A12) becomes

$$W_{\text{eff}}(q,t) = V^{\ddagger} - \tfrac{1}{2}q^2 - \tfrac{1}{2}q^3 + \tfrac{1}{2}\gamma(0)(q - a[q,t])^2. \tag{A13}$$

The position of the minimum is obtained by solving the quadratic equation $\partial W_{\text{eff}}/\partial q = 0$ which yields the two roots

$$q_{\pm}(t) = \tfrac{1}{3}[\gamma(0) - 1] \pm \sqrt{\tfrac{1}{9}[\gamma(0) - 1]^2 - \tfrac{2}{3}\gamma(0)a[q,t]}. \tag{A14}$$

From the second derivative of $W_{\text{eff}}(q,t)$, it can be seen that $q_-(t)$ is the position of the minimum while $q_+(t)$ is the position of the barrier at time t. By evaluating the second derivative of $W_{\text{eff}}(q,t)$ at $q = q_-$, the time-dependent frequency is found to be

$$\omega(t)\equiv\left[\frac{\partial^2 W_{\rm eff}}{\partial q^2}\bigg|_{q=q_-}\right]^{1/2}$$
$$=[\gamma(0)-1-3q_-(t)]^{1/2}. \qquad (\text{A15})$$

To see how well the approximate effective potential of Eq. (A12) represents the true effective potential, $q_-(t)$, computed from each of the three trajectories in Fig. 10, is plotted in Fig. 13. This plot shows that $q_-(t)$ follows the trajectory $q(t)$ extremely well. Although it is difficult to see from the two figures, there is a slight time shift between the two, i.e., $q_-(t)$ is slightly ahead of $q(t)$. This is, no doubt, the result of neglecting $\epsilon[q,t]$. However, the approximate effective potential seems to be a very good representation of the true effective potential for this case. Figure 10 also shows that the frequency of oscillation in $q(t)$ does not vary much except for the reactive trajectory. According to Eq. (A15), the frequency should not vary much unless $q_-(t)$ becomes large. For the reactive trajectory in Fig. 10, this is indeed the case, and the frequency of oscillation decreases steadily for $t>100$ as $q(t)$ goes off towards products.

The caging effect can also be understood without introducing an effective potential along the system coordinate q. Instead, one makes the observation that at large system–bath coupling strengths the system coordinate q does not coincide with the local reaction coordinate—the unbound mode—at the saddle point. Thus motion along the system coordinate q will have a large bound component orthogonal to the unbound mode, causing motion along q to be oscillatory. Below we examine the oscillatory behavior of the bound component of q for $\alpha=100$. This behavior is derived from the GLE equivalent Hamiltonian[7,8] with system coordinate q and bath modes $\{x_i\}$, by following the work of Pollak, Grabert, and Hänggi.[15,19]

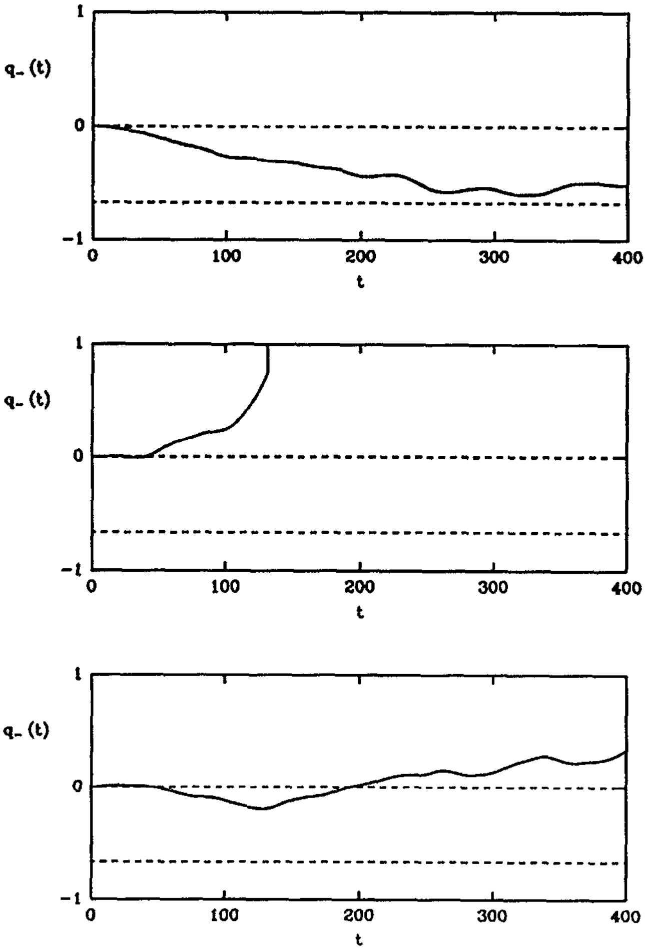

FIG. 13. The position of the minimum of the effective potential [Eq. (A14)] as a function of time corresponding to the three trajectories in Fig. 10.

The system coordinate q can be written as a linear combination of the normal coordinates, $(\rho,\{y_i\})$, of the GLE equivalent Hamiltonian used in PGH theory, i.e.,

$$q=u_{00}\rho+u_1\sigma, \qquad (\text{A16})$$

where

$$\sigma=\frac{1}{u_1}\sum_i u_{i0}y_i. \qquad (\text{A17})$$

In the limit of very large coupling strengths u_{00} is very small—for $\alpha=100$ $u_{00}=0.016$—and

$$q\approx\sum_i u_{i0}y_i. \qquad (\text{A18})$$

Thus the spectral density of the bath normal modes $\text{Re}[\hat{K}(is)]$ [Eq. (19)] can be analyzed to understand the characteristic frequency of motion exhibited by the system coordinate q. At large coupling strengths, the spectral density of the bath normal modes is dominated by the single frequency s_δ at which

$$\left[1+s_\delta^2-\alpha s_\delta\frac{2}{\sqrt{\pi}}D\left(\frac{1}{\sqrt{2}}s_\delta\tau_D\right)\right]=0, \qquad (\text{A19})$$

since

$$\text{Re}[\hat{K}(is_\delta)]=\frac{1}{\alpha u_{00}^2}e^{+(1/2)s_\delta^2\tau_D^2}, \qquad (\text{A20})$$

which, while still finite, is extremely large. For $\alpha=100$, $s_\delta=2.64$, in agreement with the observed frequency of oscillation of the trajectories $q(t)$ (Fig. 10) and in agreement with the caging analysis. The spectrum $\text{Re}[\hat{K}(is)]$ is shown in Fig. 14 for $\alpha=100$. Although it is conceptually more straightforward to introduce the GLE equivalent Hamiltonian for the above analysis, it is not necessary. The normal mode analysis can be performed directly from the GLE by following Graham,[55] and the characteristic frequency of the system coordinate is recovered.

It is instructive to consider the effective two degree of freedom (conservative) Hamiltonian used in the μVTST theory [Eq. (25)], and to see whether it can be used to predict the caging frequency. For $\alpha=100$, the saddle point region of this Hamiltonian is shown in Fig. 15. The coordinate q is represented by the dashed line. A trajectory on the two degree of freedom potential started at the saddle point with momentum along q will oscillate repeatedly with a frequency Ω as it slowly moves away from the saddle point along the very low frequency unbound mode ρ. While trajectories on this effective reduced dimensionality potential undergo the correct qualitative behavior, they oscillate with a frequency which is not observed in the simulations. For example, for

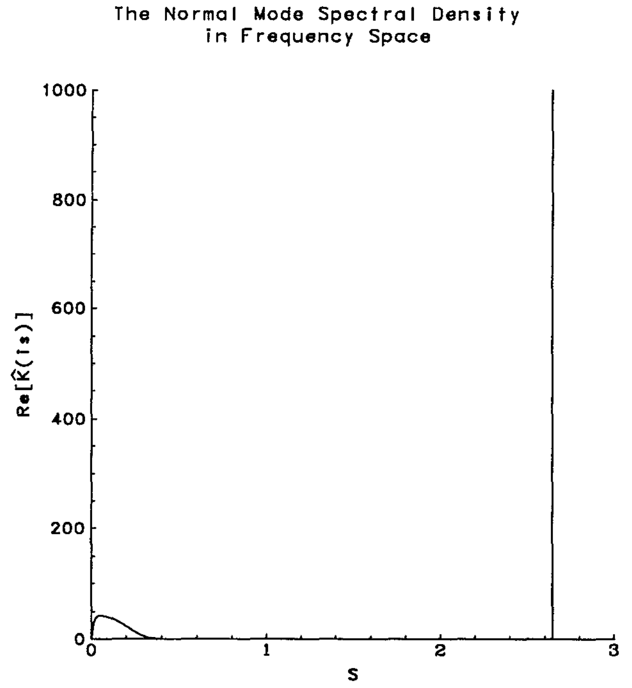

FIG. 14. The spectral density of the bath normal modes [Eq. (19)] for $\alpha = 100$, $\tau_D = 10$. Note that the maximum of the sharp high frequency peak is off scale at exp[+ 353.2]. All quantities are in reduced units, see the text.

$\alpha = 100$ the frequency $\Omega = 0.92$, which is much smaller than the observed frequency $s_\delta = 2.64$. Why is this? The collective bath mode frequency Ω [Eq. (26)] is in fact an average of all of the frequencies of the bath normal modes $\{y_j\}$. The spectral density of the bath normal modes (Fig. 14) is composed of (1) a continuum of low frequency modes which arises from the component of σ which comes from the original low frequency bath modes $\{x_j\}$, and (2) the sharp impurity peak at s_δ, which arises from the q component of σ. The average frequency Ω overemphasizes the effect of the low frequency modes, at least at very large coupling strengths.

APPENDIX B: ESTIMATE OF THE NEGLECTED ENERGY TRANSFER CONTRIBUTION TO THE μVTST RATE CONSTANT

In order to address the possibility that in the intermediate coupling regime the agreement between the μVTST ($\mathscr{X} = 0$) results and the simulation results is the fortuitous consequence of a cancellation of errors, an estimate of the neglected energy transfer contribution to the μVTST ($\mathscr{X} = 0$) rate constant is presented. The error in the μVTST ($\mathscr{X} = 0$) result is incurred by using $F_{\text{tot}}(E^\ddagger, \mathscr{X} = 0)$ [Eq. (31)] instead of $F_{\text{tot}}(E^\ddagger)$ [Eq. (29)] when evaluating $k^{\mu\text{VTST}}$ [Eq. (28)]. The error in the $\mathscr{X} = 0$ approximation is evaluated simply by calculating $k^{\mu\text{VTST}}$ from the full flux $F_{\text{tot}}(E^\ddagger)$, Eq. (29). Although evaluating $k^{\mu\text{VTST}}$ will always provide an upper bound to the rate constant, it will not necessarily provide a meaningful result if the chosen dividing surface is less than optimum. Here the pods is an optimum choice of dividing surface only for the $\mathscr{X} = 0$ case, not for the full calculation.

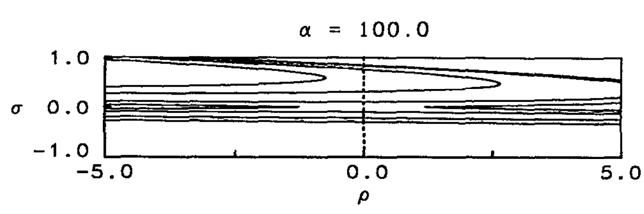

FIG. 15. Contour plot of the barrier region of the reduced two degree of freedom effective Hamiltonian [Eq. (25)] for the cubic potential [Eq. (3)] with a Gaussian friction kernel [Eq. (4)]. The dashed line is the system coordinate q [Eq. (A16)]. The decay time constant is $\tau_D = 10$ and static friction coefficient is $\alpha = 100$. Contours are at energies 0.074, 0.079, 0.10, and 0.125. All quantities are given in reduced units, see the text.

For $\alpha \lesssim 10.0$, the pods is an exceedingly poor choice of dividing surface for the energy diffusion contribution. For each of these scale factors there is an energy region within which there are three pods at each energy, as illustrated in Fig. 16 for $\alpha = 7.0$ (this is not unusual behavior, see Ref. 54). The existence of three pods per energy does not cause a difficulty in defining a single dividing surface $g(\sigma, E^\ddagger)$. At each energy the pods which gives the minimum flux is, by the variational principle, the appropriate pods to define the optimum dividing surface at that energy. In practice, this differentiation is not necessary for the $\mathscr{X} = 0$ calculation. The pods at a given energy give very similar flux contributions, and not using the pods of minimum flux does not effect the final rate constant within the accuracy quoted here.

For the full calculation including the energy diffusion contribution this differentiation is critical because the flux

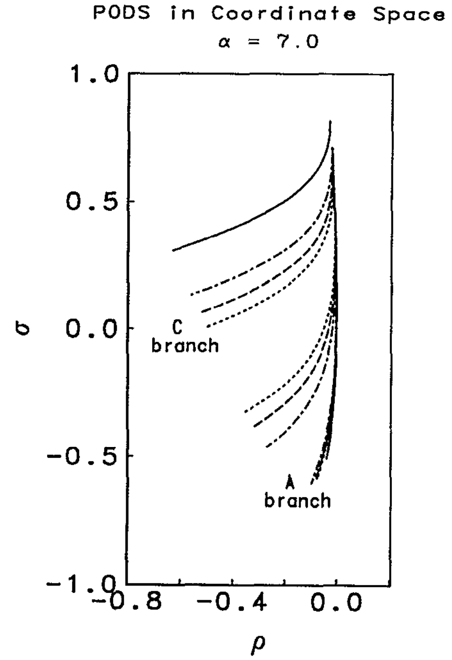

FIG. 16. Pods in the three pods per energy region for $\alpha = 7.0$. The solid lines are pods at energies $E^\ddagger = 0.077\,15$ and $E^\ddagger = 0.080\,20$, for which there exists only one pods. At each energy $E^\ddagger = 0.078\,46$ (dotted lines), $E^\ddagger = 0.078\,66$ (dashed lines), and $E^\ddagger = 0.079\,00$ (dot–dash lines), three pods are shown.

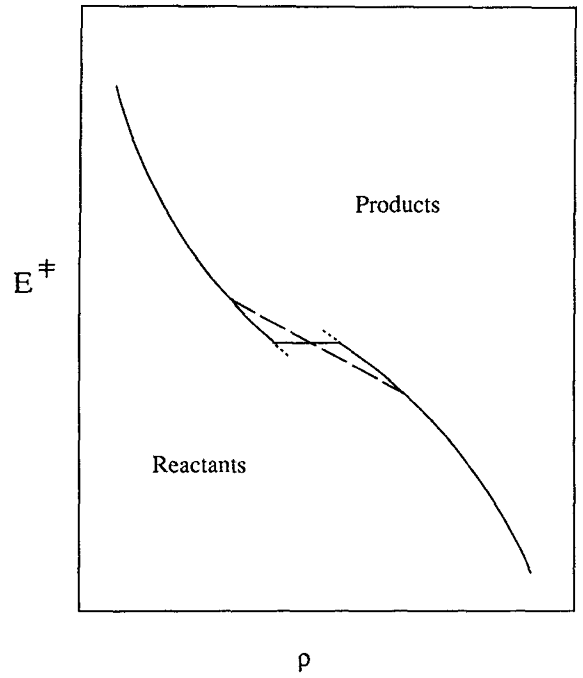

FIG. 17. A fixed sigma view of the pods as a function of energy. Dotted lines represent the continuation of the pods A and C branches beyond the dividing surface, and the dashed line is a schematic representation of a dividing surface defined to avoid a constant energy plateau.

depends upon the derivative of the pods with respect to energy, $dg/dE^{\ddagger}$. In Fig. 16, for energies less than $E^{\ddagger} \leqslant 0.0786$, the branch A pods give the lowest contribution to the flux and define the surface $g(\sigma,E^{\ddagger})$. For $E^{\ddagger} \geqslant 0.0786$, the branch C pods give the lowest contribution to the flux and define the surface $g(\sigma,E^{\ddagger})$. At $E^{\ddagger} = 0.0786$ the surface is given by a fixed energy plane (see Fig. 17). A bounded fixed energy region in $\rho,\sigma,E^{\ddagger}$ space can not be written as a path $g(\sigma)$, and a more general formalism than that presented in Eq. (29) would be necessary to evaluate the flux [see Eq. (31) of Ref. 18] through this surface. However, a planar fixed energy surface does not minimize the energy diffusion flux as required by the variational principle, rather it maximizes the energy diffusion flux. Clearly using the pods to define $g(\sigma,E^{\ddagger})$ in the full calculation will yield a gross overestimate of the energy diffusion contribution to the rate constant.

In order to get a ballpark estimate (which is still an upper bound) to the effect of neglecting the energy diffusion contribution for $\alpha \leqslant 10.0$, only the $\alpha = 10.0$ case, for which the energy diffusion contribution should be largest, is considered. For $\alpha = 10.0$ the branch A pods and branch C pods are more similar than they are at lower values of the static friction coefficients. To avoid the complication of a planar dividing surface, an approximate dividing surface is defined, as shown schematically in Fig. 17, to connect the branch A pods surface and the branch C pods surface. Calculation of $k^{\mu\mathrm{VTST}}$ with this surface yields $k^{\mu\mathrm{VTST}}/k_{\mathrm{TST}} = 0.33$ as compared to $k^{\mu\mathrm{VTST}}(\mathscr{L} = 0)/k_{\mathrm{TST}} = 0.29$. The estimated upper bound to the energy diffusion contribution at $\alpha = 10.0$ is thus 15%.

TABLE III. Ratios of rate constants.

α	$k^{\mu\mathrm{VTST}}/k_{\mathrm{TST}}$	$k^{\mu\mathrm{VTST}}_{\mathscr{L}=0}/k_{\mathrm{TST}}$	$k_{\mathrm{GLE}}/k_{\mathrm{TST}}$
10.0	0.33	0.29	0.29
14.0	0.21	0.16	0.17
20.0	0.21	0.080	0.097
100.0	0.39	0.011	0.033

For $\alpha > 14.0$, regions within which there exist three pods at each energy were not observed. For this range of static friction coefficients, calculating the total flux from the pods is straightforward. The results are presented in Table III. The $\mathscr{L} = 0$ and GLE simulation results are presented for comparison. The energy diffusion contribution increases dramatically with increasing static friction as expected. However, as the energy diffusion mechanism becomes more important, it appears that the pods become less representative of the overall optimized surface, and the total flux yields a severe overestimation of the rate constant as compared to the GLE simulation results.

[1] P. Hänggi, P. Talkner, and M. Borkovec, Rev. Mod. Phys. **62**, 251 (1990).

[2] B. J. Berne, M. Borkovec, and J. E. Straub, J. Phys. Chem. **92**, 3711 (1988).

[3] A. Nitzan, Adv. Chem. Phys. **70**, 489 (1988).

[4] J. T. Hynes, in *Theory of Chemical Reaction Dynamics*, edited by M. Baer (CRC, Boca Raton, 1985), Vol. 4, p. 171.

[5] D. G. Truhlar, W. L. Hase, and J. T. Hynes, J. Phys. Chem. **87**, 2664,5523(E) (1983).

[6] H. Mori, Prog. Theor. Phys. **33**, 423 (1965); B. J. Berne and R. Pecora, *Introduction to the Molecular Theory of Light Scattering* (Wiley, New York, 1976).

[7] R. Zwanzig, J. Stat. Phys. **9**, 215 (1973).

[8] A. O. Caldeira and A. J. Leggett, Ann. Phys. **149**, 374 (1983).

[9] B. J. Gertner, K. R. Wilson, and J. T. Hynes, J. Chem. Phys. **90**, 3537 (1989); J. P. Bergsma, B. J. Gertner, K. R. Wilson, and J. T. Hynes, *ibid.* **86**, 1356 (1987).

[10] J. P. Bergsma, B. J. Gertner, K. R. Wilson, S. Lee, and J. T. Hynes, J. Chem. Phys. **86**, 1377 (1987).

[11] J. P. Bergsma, J. R. Reimers, K. R. Wilson, and J. T. Hynes, J. Chem. Phys. **85**, 5625 (1986).

[12] J. E. Straub, M. Borkovec, and B. J. Berne, J. Chem. Phys. **89**, 4833 (1988).

[13] E. Pollak, J. Chem. Phys. **86**, 3944 (1987).

[14] B. Bagchi, Annu. Rev. Phys. Chem. **40**, 115 (1989); P. F. Barbara and W. Jarzeba, Acc. Chem. Res. **21**, 195 (1988).

[15] E. Pollak, H. Grabert, and P. Hänggi, J. Chem. Phys. **91**, 4073 (1989); H. Grabert, Phys. Rev. Lett. **61**, 1683 (1988).

[16] R. F. Grote and J. T. Hynes, J. Chem. Phys. **73**, 2715 (1980); P. Hänggi and F. Mojtabai, Phys. Rev. A **26**, 1168 (1982).

[17] H. A. Kramers, Physica **7**, 284 (1940).

[18] S. C. Tucker and E. Pollak (submitted).

[19] E. Pollak, S. C. Tucker, and B. J. Berne, Phys. Rev. Lett. **65**, 1399 (1990); E. Pollak, J. Chem. Phys. **93**, 1116 (1990).

[20] M. E. Tuckerman and B. J. Berne (work in progress).

[21] D. E. Smith and C. B. Harris, J. Chem. Phys. **92**, 1304,1312 (1990).

[22] E. Pollak, J. Chem. Phys. **95**, 533 (1991).

[23] I. Benjamin, L. L. Lee, Y. S. Li, A. Liu, and K. R. Wilson, Chem. Phys. **152**, 1 (1991).

[24] J. E. Straub, M. Borkovec, and B. J. Berne, J. Chem. Phys. **84**, 1788 (1986).

[25] M. Shugard, J. C. Tully, and A. Nitzan, J. Chem. Phys. **66**, 2534 (1977).

[26] S. O. Rice, Bell Tel. J. **23**, 282 (1944); **25**, 46 (1945).

[27] M. C. Wang and G. E. Uhlenbeck, Rev. Mod. Phys. **17**, 323 (1945).

[28] M. Berkowitz, J. D. Morgan, and J. A. McCammon, J. Chem. Phys. **78**, 3256 (1983).

[29] M. E. Tuckerman, G. Martyna, and B. J. Berne, J. Chem. Phys. **93**, 1287 (1990); M. E. Tuckerman, B. J. Berne, and A. Rossi, *ibid.* **94**, 1465 (1991); M. E. Tuckerman, B. J. Berne, and G. Martyna, *ibid.* (in press).

[30] M. Tuckerman and B. J. Berne (submitted).

[31] B. J. Berne, M. E. Tuckerman, J. E. Straub, and A. L. R. Bug, J. Chem. Phys. **93**, 5084 (1990).

[32] W. C. Swope, H. C. Anderson, P. H. Berens, and K. R. Wilson, J. Chem. Phys. **76**, 637 (1982); L. Verlet, Phys. Rev. **159**, 98 (1967).

[33] D. Chandler, J. Chem. Phys. **68**, 2959 (1978).

[34] B. J. Berne, in *Multiple Time Scales*, edited by J. U. Brackbill and B. I. Cohen (Academic, Orlando, 1985), p. 419.

[35] Generalizations of the reactive flux method for which the plateau value is normalized by something other than the conventional transition state theory rate constant have been presented in M. Borkovec and P. Talkner, J. Chem. Phys. **92**, 5307 (1990). For the simulations presented here, the velocity $\dot{q}$ at the barrier ($t = 0$) is well defined, and the conventional reactive flux method is used.

[36] H. Eyring, J. Chem. Phys. **3**, 107 (1935).

[37] E. P. Wigner, Trans. Faraday Soc. **34**, 29 (1938).

[38] V. I. Mel'nikov and S. V. Meshkov, J. Chem. Phys. **85**, 1018 (1986).

[39] B. J. Matkowsky, Z. Schuss, and E. Ben-Jacob, SIAM J. Appl. Math. **42**, 835 (1982).

[40] I. Rips and E. Pollak, Phys. Rev. A **41**, 5336 (1990).

[41] *Handbook of Mathematical Functions*, edited by M. Abramowitz and I. A. Stegun (Dover, New York, 1970), Chap. 7.

[42] E. Pollak, J. Chem. Phys. **85**, 865 (1986).

[43] N. De Leon and B. J. Berne, J. Chem. Phys. **75**, 3495 (1981); B. J. Berne, N. De Leon, and R. O. Rosenberg, J. Phys. Chem. **86**, 2166 (1982).

[44] B. J. Berne, Chem. Phys. Lett. **107**, 131 (1984).

[45] To see this, expand the potential $W(q)$ [Eq. (3)] around the well minimum at $q = -2/3$.

[46] We have seen further evidence of this regularity in surface of section plots for the effective two degree of freedom Hamiltonian for this system [Eq. (25)].

[47] Yu. Dakhnovskii and A. A. Ovchinnikov, Phys. Lett. A **113**, 147 (1985).

[48] J. C. Keck, Adv. Chem. Phys. **13**, 85 (1967); B. H. Mahan, J. Chem. Educ. **51**, 709 (1974); W. H. Miller, J. Chem. Phys. **61**, 1823 (1974).

[49] For a recent review of multidimensional transition state theory, see S. C. Tucker and D. G. Truhlar, in *New Theoretical Concepts for Understanding Organic Reactions*, NATO ASI Ser. C, edited by J. Bértran and I. G. Csizmadia (Kluwer Academic, Dordrecht, 1989), p. 231.

[50] E. Pollak, J. Phys. Chem. (in press).

[51] P. Pechukas, in *Dynamics of Molecular Collisions, Part B*, edited by W. H. Miller (Plenum, New York, 1976), Chap. 6.

[52] E. Pollak and P. Pechukas, J. Chem. Phys. **69**, 1218 (1978).

[53] P. Pechukas and E. Pollak, J. Chem. Phys. **71**, 2062 (1979).

[54] E. Pollak, in *Theory of Chemical Reaction Dynamics*, edited by M. Baer (CRC, Boca Raton, 1985), Vol. 3, p. 123.

[55] R. Graham, J. Stat. Phys. **60**, 675 (1990).